BACHELOR THESIS

Studies of the influence of the geomagnetic field on the sensitivity of gamma-ray observatories

Maria Krause

Cottbus, February 2011

Brandenburgische Technische Universität Cottbus
Politechnika Poznańska

This bachelor thesis was written at Deutsches Elektronen-Synchrotron (DESY) at its site Zeuthen.

Responsible professor: Prof. Dr. Wolfgang Lohmann

1. Supervisor: Prof. Dr. Wolfgang Lohmann
                Fakultät für Mathematik, Naturwissenschaften und Informatik
                Brandenburgische Technische Universität Cottbus
                DESY Zeuthen
                Germany
2. Supervisor: Prof. Dr. Piotr Pierański
                Wydział Fizyki Technicznej
                Politechnika Poznańska
                Poland

Abstract

Cherenkov Telescope Array (CTA) will be a ground-based high energy gamma radiation detector. This radiation is detected by the measurement of particle showers in the atmosphere. The questions of the origin of the cosmic radiation, the functional principle of cosmic particle accelerators in the area of black holes or the nature of the dark matter are in the scientific goals of CTA. At the moment the instrument is in the planning phase and first results will probably be in 2014.

The site of the instrument has an immediate influence on the sensitivity e.g. due to the weather, the height above sea level. Several possible sites for CTA are being considered at the moment including Namibia, Argentina, Canary islands and Mexico. The geomagnetic field affects the development of showers and distorts the images of the air shower in the telescope. The aim of this work is to quantify the influence of the strength and the direction of the geomagnetic field at the different possible locations on the sensitivity of CTA using Monte Carlo simulations of particle showers. Firstly, we simulated the lateral distribution at the twelve sites. The geomagnetic field of the sites was obtained from the National Geographic Data Center (NGDC). To study the influence of the Earth's magnetic field, we held the altitude of the sites constant at 2000 m. Hence, we could choose two sites per hemisphere which could be potential candidates for the Cherenkov Telescope Array: Beaufort West (South Africa), El Leoncito (Argentina), La Palma (Canary Islands) and San Pedro Martir (Mexico). To compare the results with a site which is already known, we chose the observatory H.E.S.S. in Namibia. After the study of the energy thresholds and the effective areas we decided in favour of two sites, one in the southern and one in the northern hemisphere. Considering the influence of the geomagnetic field on the predictions, the southern observatory should be in Beaufort West in South Africa. The northern array of CTA would be on the Canary Island La Palma. The disadvantages of the candidate sites with a large influence of the geomagnetic field are compensated with a higher altitude of the locations. After the investigation of the Cherenkov light characteristics, the energy spectra and the corresponding effective areas, we chose one place for the southern array and one place for the northern array of CTA: El Leoncito in Argentina and San Pedro Martir in Mexico.

Zusammenfassung

Das Cherenkov Telescope Array (CTA) ist ein bodengebundenes Gammastrahlen-Teleskop zur Vermessung des nichtthermischen Universums im Energiebereich oberhalb von 20 GeV. Die Fragen nach dem Ursprung der kosmischen Strahlung, der Funktionsweise kosmischer Teilchenbeschleuniger in der Umgebung von schwarzen Löchern oder der Natur der dunklen Materie stehen im wissenschaftlichen Blickpunkt von CTA. Das Instrument befindet sich zurzeit in der Planungsphase und wird voraussichtlich ab 2014 erste wissenschaftliche Daten liefern.

Der Standort des Instruments hat unmittelbaren Einfluss auf die Sensitivität wie z.B. durch das Wetter oder die Höhe über dem Meeresspiegel. Mehrere mögliche Standorte für CTA werden zurzeit charakterisiert (Namibia, Argentinien, Kanarische Inseln oder Mexiko). Ziel dieser Arbeit ist es, den Einfluss der Stärke und Richtung des Erdmagnetfeldes an den verschiedenen möglichen Standorten auf die Sensitivität von CTA durch Monte Carlo Simulationen von Teilchenschauern zu quantifizieren. Das geomagnetische Feld wurde aus Messungen des National Geographic Data Centers (NGDC) für jeden Standort erhalten. Ausgewertet wurde die Verteilung der Cherenkov Photonen am Boden. Um die Einflüsse des Erdmagnetfeldes besser zu erkennen, wurden die Höhen der verschiedenen Standorte zunächst konstant auf 2000 m gehalten. Aufgrund der Simulationen der Lateralverteilungen der Cherenkov Photonen wurden je zwei Orte auf der Nord- und Südhalbkugel bestimmt, welche potenzielle Kandidaten für das Cherenkov Telescope Array sind: Beaufort West (Südafrika), El Leoncito (Argentinien), La Palma (Kanarische Inseln) und San Pedro Martir (Mexiko). Für den Vergleich mit eines schon untersuchten Standortes wurde das Observatorium H.E.S.S. in Namibia gewählt. Nachdem die Energiespektren, deren Energieschwellen und die jeweiligen effektiven Flächen der vier ausgewählten Standorte untersucht wurden, haben wir uns für je einen Ort auf der Nord- und Südhalbkugel entschieden. Unter Berücksichtigung der Simulationen der Verteilung der Cherenkov Photonen am Boden und des Einflusses des geomagnetischen Feldes sollte das südliche Observatorium in Beaufort West in Südafrika liegen. Die nördliche Anordnung des Gammateleskop würde demnach auf der Kanarischen Insel La Palma gebaut werden. Allerdings werden die Nachteile, die durch einen hohen

Einfluss des geomagnetischen Feldes entstehen, durch zunehmende Höhe kompensiert. Aufgrund der vorausgesagten Teilchendichte am Boden, der Energiespektren sowie der Energieschwellen und der dazugehörigen effektiven Flächen auf den jeweiligen Höhen, kommen wir schließlich zu dem Ergebnis, dass sich der südliche Teil von CTA bei El Leoncito in Argentinien und der Nördliche bei San Pedro Martir in Mexiko befinden sollte.s geomagnetische Feld wurde aus Messungen des National Geographic Data Centers (NGDC) für jeden Standort erhalten. Ausgewertet wurde die Verteilung der Cherenkov Photonen am Boden. Um die Einflüsse des Erdmagnetfeldes besser zu erkennen, wurden die Höhen der verschiedenen Standorte zunächst konstant auf 2000 m gehalten. Aufgrund der Simulationen der Lateralverteilungen der Cherenkov Photonen wurden je zwei Orte auf der Nord- und Südhalbkugel bestimmt, welche potenzielle Kandidaten für das Cherenkov Telescope Array sind: Beaufort West (Südafrika), El Leoncito (Argentinien), La Palma (Kanarische Inseln) und San Pedro Martir (Mexiko). Für den Vergleich mit eines schon untersuchten Standortes wurde das Observatorium H.E.S.S. in Namibia gewählt. Nachdem die Energiespektren, deren Energieschwellen und die jeweiligen effektiven Flächen der vier ausgewählten Standorte untersucht wurden, haben wir uns für je einen Ort auf der Nord- und Südhalbkugel entschieden. Unter Berücksichtigung der Simulationen der Verteilung der Cherenkov Photonen am Boden und des Einflusses des geomagnetischen Feldes sollte das südliche Observatorium in Beaufort West in Südafrika liegen. Die nördliche Anordnung des Gammateleskop würde demnach auf der Kanarischen Insel La Palma gebaut werden. Allerdings werden die Nachteile, die durch einen hohen Einfluss des geomagnetischen Feldes entstehen, durch zunehmende Höhe kompensiert. Aufgrund der vorausgesagten Teilchendichte am Boden, der Energiespektren sowie der Energieschwellen und der dazugehörigen effektiven Flächen auf den jeweiligen Höhen, kommen wir schließlich zu dem Ergebnis, dass sich der südliche Teil von CTA bei El Leoncito in Argentinien und der Nördliche bei San Pedro Martir in Mexiko befinden sollte.

Table of Contents

List of Figures

List of Tables

List of Abbreviation and Symbols

Abbreviations

a.s.l.	above sea level
AZ	Azimuth
CANGAROO	Collaboration of Australia and Nippon (Japan) for a GAmma Ray Observatory in the Outback
CORSIKA	COsmic Ray SImulations for KAscade
CPU	Central Processing Unit
CTA	Cherenkov Telescope Array
DESY	Deutsches Elektronen SYnchrotron
EAS	Extensive Air Showers
EM	Electromagnetic
EGS4	Electron Gamma Shower system version 4
FoV	Field Of View
H.E.S.S.	The High Energetic Stereoscopic System
HEGRA	High Energy Gamma Ray Astronomy
IACT	Imaging Atmospheric Cherenkov Technique
KASCADE	Karlsruhe Shower Core and Array DEtector
MAGIC	Major Atmospheric Gamma-ray Imaging Cherenkov Telescope
MC	Monte Carlo (simulations)
PMT	Photomultiplier Tube
ROOT	An Object-Oriented Data Analysis Framework
VERITAS	Very Energetic Radiation Imaging Telescope Array System
VHE	Very High Energy
ZE	Zenith

Symbols

Particles

γ	Photon
e^-	Electron
e^+	Positron

Physical constants

α	Fine-structure constant	$e^2/4\pi\epsilon_0\hbar c \approx 1/137$
c	Speed of light in vacuum	$299792458 \; \frac{m}{s}$
		In natural units $c = 1$, hence the mass, the momentum and the energy are given in units of eV.
e	Electron charge magnitude	$1.602176487 \cdot 10^{-19} \; C$
$\hbar$	Planck constant, reduced	$\hbar = h/2\pi = 1.054571628 \cdot 10^{-34} \; Js$
		$= 6.58211899 \cdot 10^{-22} \; MeVs$
		In natural units $\hbar = 1$.
m_e	Electron mass	$9.10938212 \cdot 10^{-31} \; kg = 0.510998910 \; \frac{MeV}{c^2}$
μ_0	Permeability of free space	$4\pi \cdot 10^{-7} \frac{N}{A^2}$
N_A	Avogadro constant	$6.02214179 \cdot 10^{23} \; mol^{-1}$
r_e	Classical electron radius	$2.8179402894 \cdot 10^{-15} \; m$
r	Earth mean equatorial radius	$6.378137 \cdot 10^6 \; m$

Chapter 1

Introduction

1.1 What is gamma-ray astronomy?

Gamma-ray astronomy is the study of photons from space with an energy range from about 100 keV to > 100 EeV (10^{20} eV). This is a range of more than 15 decades. Hence, to cover this huge band a wide variety of detection techniques is necessary. This thesis will concentrate on the gamma-ray band above a few 10^{10} eV, the Very High Energy, VHE, γ-astronomy. The main goal of gamma-ray astronomy is to explore the production and propagation of VHE γ-rays in the universe. Sources of VHE γ-rays are supernovae remnants, pulsars, active galactic nuclei or binary systems such as microquasars. About 20 years ago the research of VHE gamma-ray astronomy started with the first observation of the Crab Nebula by the Whipple observatory. The detection technique of VHE is the measurement of the resulting electromagnetic cascade developed in the Earth's atmosphere. In contrast to charged cosmic rays, neutral particles point back to the location of their origin because charged particles will be deflected by the magnetic field of the universe [1, 2].

1.2 Radiation processes

A very high energetic primary particle which hits the atmosphere initiates a cascade of secondary particles that strike towards the Earth, this is called an *Extensive Air Shower* which will be described in Section 1.3.1. During the travel of the particles through the atmosphere different radiation processes take place. At this point we will briefly describe the processes which are considered for our study.

Pair production

Pair production is the most important absorption mechanism for VHE gamma rays. This interaction occurs when a photon with an energy

$$E > 1.02 \; MeV = 2m_e c^2 \tag{1.1}$$

interacts with the electromagnetic field of a nucleus of charge Z, where m_e is the electron mass and c the speed of light in vacuum. The incident gamma annihilates and its energy is transferred to an electron-positron-pair (e^--e^+-pair):

$$\gamma + Z \rightarrow e^+ + e^- + Z \tag{1.2}$$

Figure 1.1 shows the process of pair production. If pair production occurs, the photon energy is converted into rest mass and kinetic energy of the electron-positron pair. The direction of the incident photon can be inferred by the trajectories of the produced e^+ and e^-. The kinetic energy of the gamma ray is not equally shared between electron and positron and the initial direction is not necessarily the mean of their emission angles. The cross section of the pair production ($\sigma_{pp} \sim Z^2 \ln E_\gamma$) increases as the photon energy increases and approaches an asymptotic value. An important property of particle motion is the mean free path which is the average distance of a moving particle before it undergoes an interaction which modify its direction or energy. The value of mean free path for the pair production is related to the radiation length X_0 which is defined in the next chapter [1, 3]:

$$\lambda_{pp} = \frac{9}{7} X_0. \tag{1.3}$$

Electron bremsstrahlung

Electron bremsstrahlung is the radiation process when an incident charged particle, such as an electron, is deflected in the electric field of a nucleus. Hence, it emits electromagnetic radiation whose amplitude is proportional to the acceleration which is generated by the deflection. The radiation is produced by charged particles (electrons) passing through a specific medium. In particular, radiation which is caused by the deceleration in the field of atomic nuclei is called external bremsstrahlung (Figure 1.1). Bremsstrahlung dominates the energy loss of electrons and positrons above the critical energy, E_c, being the energy at which the main energy loss mechanism changes from radiation losses such as bremsstrahlung to ionization losses. The energy loss via bremsstrahlung is given as [3, 4, 5]:

$$-\frac{dE}{dx} = 4\alpha N_A \frac{Z^2}{A} z^2 r_e^2 E \ln \frac{183}{Z^{1/3}}, \tag{1.4}$$

where

α - Fine-structure constant

N_A - Avogadro constant

Z - Atomic number of absorber

z - Charge of incident particle

A - Atomic mass of absorber

r_e - Classical electron radius

E - Energy of incident particle

For the energy E after a path length x follows:

$$-\frac{dE}{dx} = \frac{E}{X_0} \tag{1.5}$$

and after integration

$$E(x) = E_0 e^{\frac{x}{X_0}} \tag{1.6}$$

The radiation length X_0 is the distance over which the energy of a high-energy electron decreases due to bremsstrahlung by a factor of $1/e$ [1].
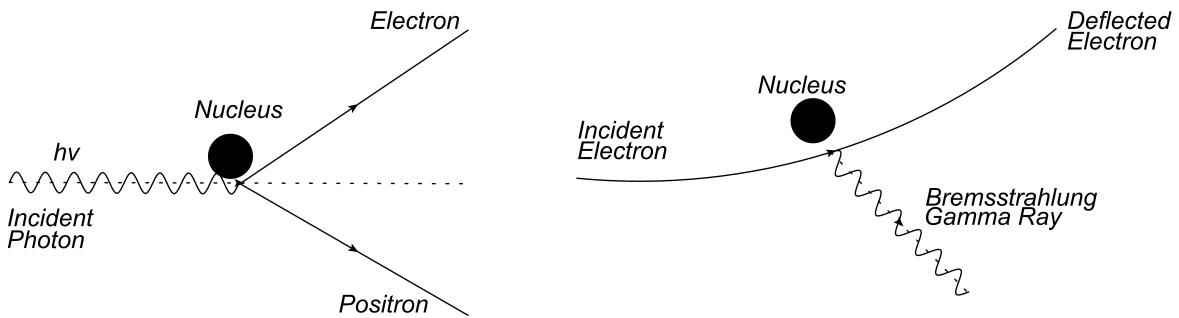
Figure 1.1: Radiation processes.
Right: pair production; left: electron bremsstrahlung [1, 6].

Coulomb scattering

Another process which is important for understanding extensive air showers, EAS, is the Coulomb scattering. The charged particle which traverses a medium is deflected by elastic collisions in the Coulomb field of nuclei. The nuclei are normally much more massive than the scattered particles,

---

[1]Here e denotes Euler's number.

therefore the direction of flight might be changed but not the absolute value of the energy. The angle between the initial and scattered direction is very small. The Coulomb scattering distribution is well described by the Molière theory [6, 7].

1.3 Experimental Basics

1.3.1 Extensive Air Showers

An EAS (Figure 1.2) is a particle shower initiated by a very high energy particle of energy larger than 100 MeV which hits the top of the atmosphere. EAS are cascades with an electromagnetic, a muonic, a hadronic and a neutrino component. If the primary particle is a photon nearly only electromagnetic interactions take place which we will focus on. The first interaction takes place about 20 km above the Earth's surface, the photon converts into an electron and a positron on the top of the atmosphere. Electron and positron produce again photons via bremsstrahlung in the Coulomb field of the nuclei that comprise the atmosphere and hence an electromagnetic cascade is started. The particle shower spreads out because of the interaction with the molecules in the air due to Coulomb scattering as well as the deflection angles of pair production and bremsstrahlung. The number of electrons, positrons and photons in the shower increases as a function of atmospheric depth. Eventually the rate of ionization energy loss exceeds that of bremsstrahlung. Therefore, the shower electrons lose all of their energy before they are able to produce secondary gamma ray, and the shower development begins to fall off. For energies above 100 MeV, the electrons lose almost all energy through bremsstrahlung. The secondary charged particles in the EAS with a speed greater than the speed of light in the medium (in our case: air) emit Cherenkov light which can be detected using a Cherenkov telescope array. Consequently, we get information about the original photon. This method is called Imaging Atmospheric Cherenkov Technique.
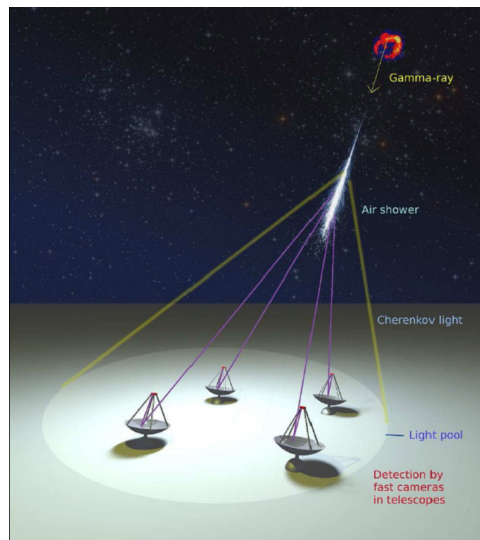
Figure 1.2: Production of extensive air showers [8].

The process of an electromagnetic cascade is shown in Figure 1.3 schematically. A very simple model of EM cascade development was presented by Walter Heinrich Heitler (1904-1981) who was a German physicist [9]:
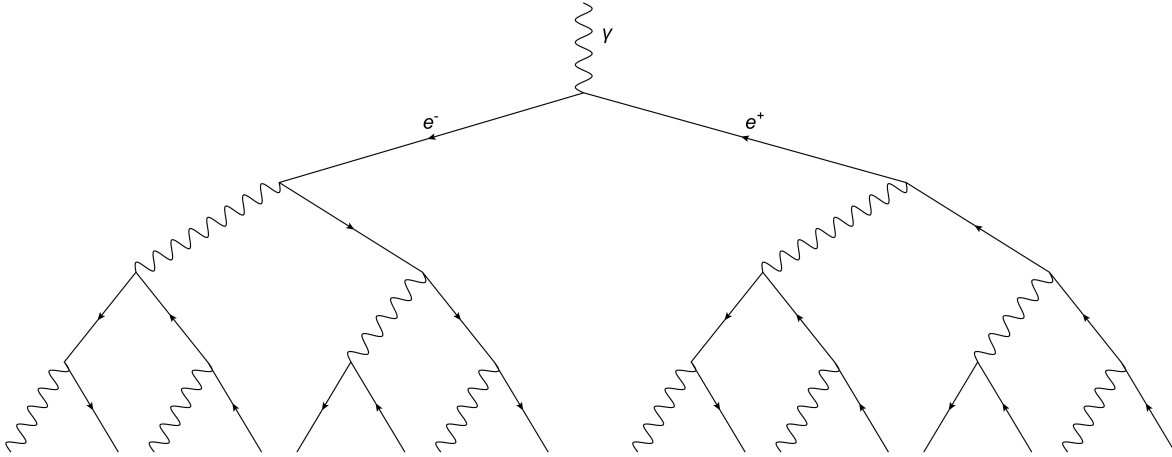
Figure 1.3: Schematic diagram of a photon initiated electromagnetic shower.

As we could see in the figure an electron [2] radiates a single photon after traveling a certain length d which is set to the length over which an electron loses half its energy by radiation:

$$d = X_0 \ln 2, \tag{1.7}$$

After traveling the same distance, a photon undergoes pair production again. The energy of a particle is assumed to be equally divided between two outgoing particles. After a distance

$$x = n X_0 \ln 2, \tag{1.8}$$

the total number of particles in the shower, containing electrons, positrons and photons, is

$$N = 2^n = e^{\frac{x}{X_0}}, \tag{1.9}$$

where n is the number of radiation lengths. Since the energy is distributed to more particles with each step of the cascade, the mean energy of a particle decreases with every step. After several steps, the energy of the photons are too low to produce new e^+e^--pairs; this energy is the critical energy E_c which is in air about 85 MeV. Thereby the electromagnetic shower dies out due to ionisation energy-loss of the particles with the air [9, 10]. The energy of the primary photon can be calculated with the maximum shower size N_{max}:

$$E_0 = E_c N_{max}. \tag{1.10}$$

The penetration depth X_{max} at which the EM shower reaches its maximum size after n_c splitting lengths is calculated to:

$$N_{max} \underset{1.9}{=} 2^{n_c}$$

$$E_0 \underset{1.10}{=} E_c N_{max}$$

$$X_{max} \underset{1.8}{=} n_c X_0 \ln 2$$

$$X_{max} \underset{1.9,1.10}{=} \ln \left(\frac{E_0}{E_c} \right) X_0. \tag{1.11}$$

The radiation length X_0 in air is 36.6 g/cm^2. The density profile of the atmosphere is described by a slab model [10] where the variation in pressure on each side of a vertical slab of atmosphere must balance the downward gravitational force on the slab:

$$\rho = \rho_0 e^{-\frac{z}{h}}, \tag{1.12}$$

where $\rho_0 \approx 1.205 \times 10^{-3} g/cm^3$ is the typical atmosphere density at sea level, z is the height a.s.l. and

---

[2]electron=positron

$h \approx 8.5\ km$ is the scale height of the atmosphere. Layers used to describe the atmosphere include the troposphere (0 km to 17 km (tropics)), stratosphere (between 17 km and 50 km), mesosphere (between 50 km and 85 km), thermosphere (between 85 km and 500 km) and exosphere (higher than 500 km). We can say the higher the altitude above sea level, the thinner the atmosphere, the smaller the density [10].

1.3.2 Cherenkov radiation

The Cherenkov phenomenon was discovered by Pavel Alekseyevich Cherenkov (1904-1990), and theoretically understood by Russian Ilya Mikhailovich Frank (1908-1990) and Igor Yevgenyevich Tamm (1895-1971). They received the Nobel Prize for Physics in 1958 for their discovery and interpretation of the Cherenkov effect in 1934. Cherenkov radiation is emitted when charged particles pass through matter with a velocity v which is higher than the velocity of light in the medium:

$$\frac{v}{c} > \frac{1}{n},\tag{1.13}$$

where c is the velocity of light in a vacuum and n is the refractive index. The Cherenkov radiation is emitted within an angle Θ_C (Cherenkov angle) with respect to the direction of the charged particle, as shown in Figure 1.4, and depends on the refractive index.
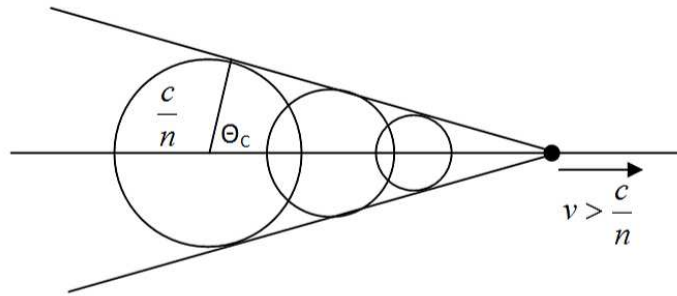
Figure 1.4: Schematic diagram of the Cherenkov angle emitted by a charged particle.

During the flight of a charged particle through the dielectric medium, it interacts electrically with the molecules in its vicinity. At low velocity, which means $v < c$, the disarrangement of the polarization field is symmetrical around and along the particle trajectory, as in Figure 1.5(a). There is no residual electric field and thus, no measurable radiation. Otherwise, if the velocity of the charged particle through the dielectric medium exceeds the velocity of light in the medium (Figure 1.5(b)), the neutrality of the molecules is disturbed. It occurs an induced polarization and hence the molecules turns on and off as the particle passes. That is the reason why the molecules radiate and photons are emitted [1].

The Cherenkov equation shows the relation between the refractive index n and the angle Θ_C which can be calculated using v and n:

$$cos\Theta_C = \frac{c}{n(z_h)v} = \frac{1}{n(z_h)\beta},\tag{1.14}$$

where z_h is the height above sea level. With the help of this relation we can outline many important properties:

- There is a threshold velocity for a medium of a given refractive index n

$$\frac{v}{c} = \beta = \frac{1}{n} \qquad (1.15)$$

  below which no radiation occurs.

- The maximum angle of emission takes place when $v = c$ respectively $\beta = 1$: $cos\Theta_C = 1/n$.
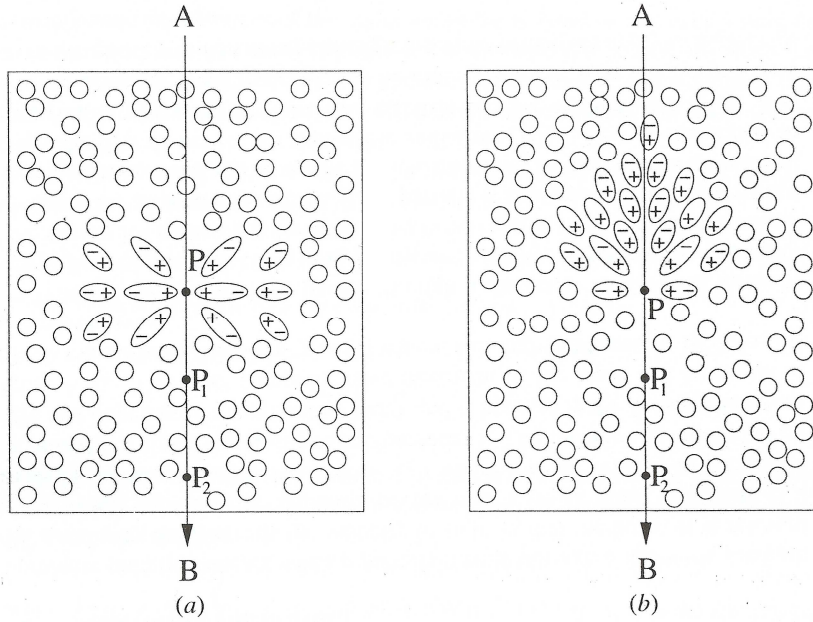
Figure 1.5: The polarisation set up in a dielectric medium by the passage of a charged particle when $v < c$ (a) and $v > c$ (b) [1].

The refractive index is the critical parameter to characterise the physics of Cherenkov radiation. It is convenient to introduce a parameter η parametrized as $\eta = n - 1$; then η is proportional to the density of air [10]:

$$\eta \approx \eta_0 e^{\left(-\frac{z_h}{h_0}\right)}, \qquad (1.16)$$

where $\eta_0 = 2.9 \cdot 10^{-4}$ and $h_0 = 7250 \ m$ which is slightly different from the atmospheric standard scale height [10, 11]. The Cherenkov angle at sea level ($z_h = 0$) for an EM shower traveling through the atmosphere with $\beta = 1$ and $n = 1.00029$, calculated with equation (1.16), is

$$\Theta_C = \arccos\left(\frac{1}{n(z_h)\beta}\right)$$

$$= \arccos\left(\frac{1}{(\eta_0 e^{\left(-\frac{z_h}{h_0}\right)} + 1)\beta}\right) \qquad (1.17)$$

$$\Theta_C = 1.38°.$$

The number of produced Cherenkov photons by a charged particle is described by the Frank-Tamm formula. The equation describes the amount of Cherenkov radiation emitted per unit path length dx in the wavelength interval $[\lambda_1, \lambda_2]$ at Cherenkov angle Θ_C. In our case we simulated a spectrum from 250 nm to 700 nm because the absorption in the atmosphere and the spectral sensitivity of the

photomultiplier tubes of the telescope cameras make detection below a wavelength of 250 nm difficult.

$$\frac{d^2N}{d\lambda dx} = \frac{2\pi\alpha z^2}{\lambda^2}\sin^2(\Theta_C)$$

$$\frac{dN}{dx} = \int\limits_{250\ nm}^{700\ nm} \frac{d^2N}{d\lambda dx}d\lambda$$

$$= \int\limits_{250\ nm}^{700\ nm} \frac{2\pi\alpha z^2}{\lambda^2}\sin^2(\Theta_C)d\lambda$$

$$= 2\pi\alpha z^2\sin^2(\Theta_C)\left[-\frac{1}{\lambda}\right]_{250\ nm}^{700\ nm}$$

$$\frac{dN}{dx} \approx 393 z^2\sin^2(\Theta_C)\frac{Photons}{cm}.$$

As can be seen, the number of Cherenkov photons depends on the charge of the particle and the Cherenkov angle.

1.3.3 Geomagnetic field

Finding the best site for the Cherenkov Telescope Array, CTA, is currently being investigated; CTA will be introduced in more detailed in the next section. There are a lot of facts which are important to find the best location, including the geomagnetic field which is different in various places of the Earth. Our planet operates like a sphere with a dipole inside which is surrounded by a magnetic field. The axis of the dipole is offset from the axis of the Earth's rotation; the difference in angle is about 11° which means that the north and south magnetic poles are not in the same place as the geographic north and the south poles. In 2010, the north magnetic pole is located at 84.97°N and 132.35°W and the south magnetic pole at 64.42°S and 137.34°E. The magnetic field lines pass out in the southern hemisphere and enter the Earth in the northern hemisphere. The geomagnetic field is variable in time and space. It is measured to high precision by satellite instruments. There are over 200 magnetic observatories worldwide [12]. At any point and time, the geomagnetic field is characterised by a direction and intensity. If we measure the magnetic declination D, the horizontal intensity H and the vertical intensity Z, the components of the vector of the geomagnetic field, all parameters of the geomagnetic field listed below can be calculated. By convention, the total magnetic field is described by seven parameters, as sketched in Figure 1.6:

- Declination (D)

- Inclination (I)

- Horizontal intensity (H)

- North component of the horizontal intensity (X)

- East component of the horizontal intensity (Y)

- Vertical intensity (Z)

- Total intensity (F)

These seven parameters are frequently used but not all needed to describe the geomagnetic field. The declination D and the inclination I describe the direction of the field. The horizontal H, vertical Z, the north X and east Y components of the horizontal intensity characterise the total intensity F of the magnetic field. Figure 1.7 illustrates the intensity of the geomagnetic field on the world including the position of candidate sites (yellow dots). This field variates between a value of approximately 20000 nT and 70000 nT. A very important component is the declination which plays an interesting role in the definition of the direction of the geomagnetic field. It is the angle between the magnetic

and the true north. The declination is positive when the magnetic north is east of true north. For example, the declination of San Pedro Martir (Mexico) is 11.5° which means that a compass at that location which points north (magnetic) would actually align 11.5°E of true north. We could say that 11.5°E would indicate that magnetic north lies 11.5° clockwise from true north. The inclination I is the angle between the magnetic field vector and the horizontal plane which is tangent to the Earth's surface at that point [12], positive down and negative up.

The momentum of a charged particle p is measured with a magnetic field B which forces the charged particle to move on a helix due to the Lorentz force. The radius of the helix r_g, the so called gyroradius (Lamor radius), can be calculated with the centripetal and the Lorentz force:

$$F_Z = F_L$$
$$r_g = \frac{p}{qB}. \tag{1.18}$$

The magnetic rigidity R is the amount of resistance of a charged particle to deflection by a magnetic field:

$$R = \frac{p}{q} = r_g B. \tag{1.19}$$

The geomagnetic field is very inhomogeneous [13, 14]. In a first approximation, the Earth's magnetic field can be described as an ideal dipole:

$$B(r, \lambda) = \frac{\mu_0}{4\pi} \frac{p_m}{r^3} \sqrt{1 + 3 \sin^2 \lambda} \tag{1.20}$$

where

$p_m \approx 8.1 \cdot 10^{22} Am^2$ - Magnetic dipole moment

$r = 6378 \ m$ - Earth mean equatorial radius

$\mu_0 \approx 4\pi \cdot 10^{-7} \ T \cdot m/A$ - Permeability of free space

Equation 1.20 includes the magnetic latitude λ which is 0° for a location at the equator and counted northwards. At the north pole, the magnetic latitude is 90° and at the south pole −90°. Consequently the magnetic field is 31.32 μT for a location at equator ($\lambda = 0$).
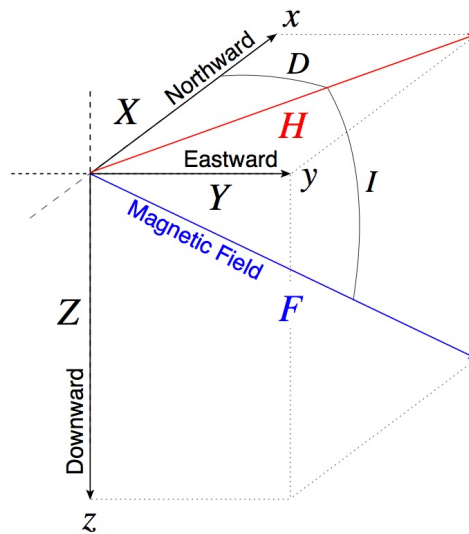
Figure 1.6: The seven parameters of the geomagnetic field [12].
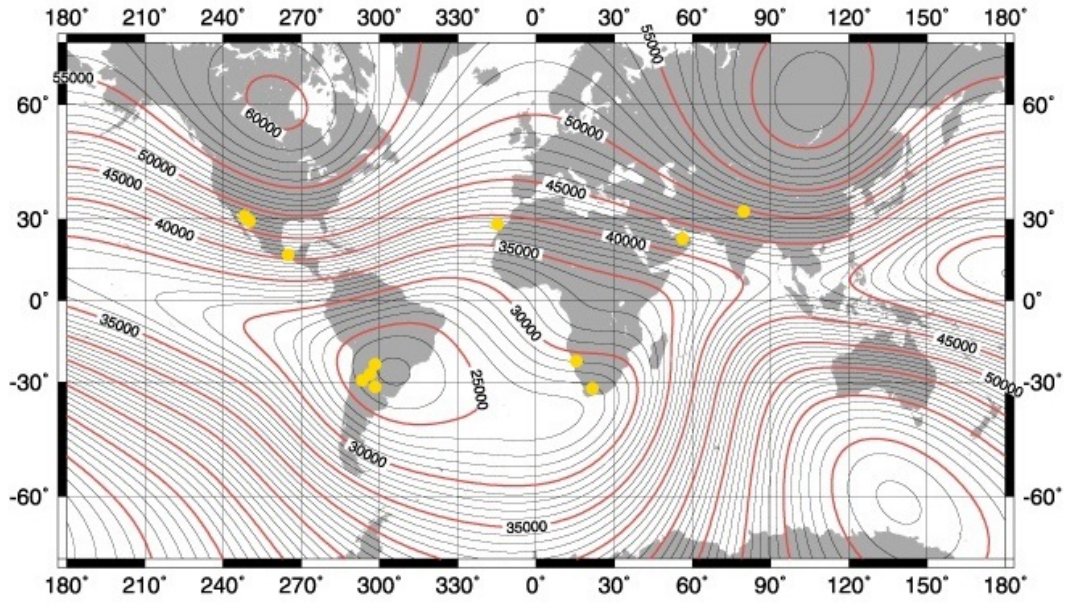
Figure 1.7: Isobars of the total intensity - main field (in nT) measured by the National Geophysical Data Center [12] including the position of candidate sites (yellow dots).

Chapter 2

Cherenkov Telescope Array

Cherenkov Telescope Array (CTA) will be a ground-based high energy gamma-ray observatory which will study astrophysical sources in an energy range from 10 GeV to about 100 TeV. It will allow deeper investigations of galactic sources, the central part of the milky way and the observation of extragalactic objects like pulsars and microquasars. Current instruments used in gamma-ray astronomy are Whipple, CANGAROO, H.E.S.S., MAGIC, MILAGRO and VERITAS [15]. At the moment the instrument is in the planning phase. *First light* will be in 2014.

2.1 Scientific goals

The aims of CTA are to find the origin of cosmic rays and dark matter as well as to find physics beyond the standard model of particle physics. CTA will advance the state of the art in astronomy and astrophysics at the highest energies of the electromagnetic spectrum. The performance of the instrument is superior with respect to previous ones and it will be operated as an open observatory. There will be a support for easy access and analysis of data. The observatory will be open to the entire community of astrophysics. Science performance goals for CTA include in particular the improvement of the sensitivity, energy range, angular resolution, temporal resolution, flexibility, survey capability, number of detected sources and the global coverage and integration. CTA wants to observe in a wide energy range of the electromagnetic spectrum from below 10 GeV to above 100 TeV to understand the physical processes in sources of high-energy radiation. This should be done with about a factor 10 more sensitivity on gamma-ray sources than any existing instrument. CTA will improve the angular resolution down to the range of arc-minutes which is a factor of 5 better than the typical value for current telescopes. The large detection area will help to resolve flaring and time-variable emission on sub-minute time scales which is only reachable for the strongest sources with current instruments. Another advantage of the large number of individual telescopes is the number of different configurations which allow different operating modes. Thus, the survey capability enhances dramatically because some groups of telescopes of the array can point to adjacent fields in the sky. As a consequence, their fields of view overlap and provide an increase of the covered sky area, enabling a survey at high sensitivity. As a result, the number of detected sources will increase [16]. Quoted according to the CTA consortium [16], global coverage and integration will be realized because

> „CTA aims to provide full sky coverage from multiple observatory sites, using transparent access and identical tools to extract and analyse data.“

.

2.2 Array layout

The observatory will consist of two arrays, each with 50 to 100 telescopes in the northern and southern hemisphere. There should be three different types of telescopes in each array in order to cover a wide energy range from about 10 GeV to about 100 TeV. In comparison to the southern array, the instruments in the northern hemisphere will just cover an energy range from some 10 GeV to greater than 1 TeV while the telescopes of the southern part will work at an energy range up to 100 TeV [16]. The southern array will cover the central part of the galactic plane and see mostly galactic sources e.g. pulsars, binary systems, supernovae remnants or pulsar wind nebulae. As a result, it needs to be sensitive over the full energy range. On the other hand the northern array will be designed for extragalactic astronomy such as active galactic nuclei, gamma-ray bursts or other extragalactic sources

and will not observe at the highest energies. To detect particle showers down to a few 10 GeV the Cherenkov light needs to be sampled and detected efficiently. The CTA consortium assumes a few very large telescopes with a diameter of about 20 to 30 m. The arrangement of this part of the array can be in a few 10000 m^2. The smaller in size telescopes will cover the energy range from about 100 GeV to about 10 TeV with a grid of telescopes of 10 to 15 m with a spacing of about 100 m. The telescope array for the high-energy range will detect gamma-ray showers above 10 TeV at an array which will cover an area of several km^2. There will be a large number of small telescopes with a dish area of a few m^2 and a spacing of 100 to 200 m [15, 16], as illustrated in Figure 2.1.
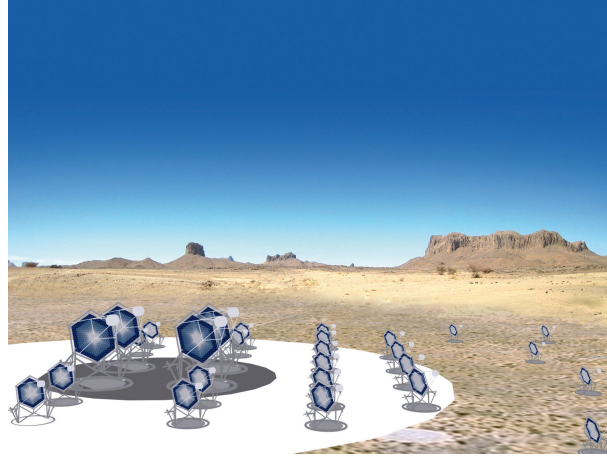
Figure 2.1: Artist's model of the Cherenkov Telescope Array [17].

2.3 Candidate sites

The selection of the sites is very important for the achievement of an optimum performance and scientific output [16]. There are different criteria which have to be considered. These include for example the geographical, observational and environmental conditions, questions of logistics, accessibility, availability, stability of the host region and local support. In the following the geographical conditions are described. The description of the other conditions is well documented in [16]. Having the best sky coverage, the latitude of the sites should be between 30° north and 30° south and the altitude should be from about 1500 m to 4000 m. It is crucial that the locations have reasonable flat areas of at least 10 km^2 in the southern hemisphere and about 1 km^2 in the northern hemisphere. Having a low component of the geomagnetic field parallel to the surface is desirable because this field deflects air shower particles. The table below lists the possible locations for CTA with their latitudes, longitudes, altitudes, declinations, horizontal and vertical field intensities. These data were taken from the 11th Generation International Geomagnetic Reference Field (IGRF11).

Site	Latitude	Longitude	Altitude [m]	Declination	Inclination	Horizontal Intensity [μT]	Vertical Intensity [μT]	Total Field [μT]
ALMA (Argentina)	22°59'56"S	67°45'39"W	5000	- 4.7°	-20.22°	21.697	-7.991	23.121
H.E.S.S.	23°16'18"S	16°30'00"E	1800	-13.62°	-64.62°	12.190	-25.684	28.429
Salar de Pocitos (Argentina)	24°26'40"S	67°06'10"W	3650	-4.72°	-22.37°	21.266	-8.860	23.038
El Leoncito (Argentina)	31°44'11"S	69°16'39"W	2600	0.7°	-31.83°	20.179	-12.529	23.753
La Silla (Chile)	29°15'00"S	70°43'48"W	2400	0.7°	-28.57°	20.815	-11.336	23.702
Beaufort West (South Africa)	32°28'48"S	22°14'60"E	1750	-24.07°	-65.38°	11.023	-24.065	26.469
La Palma	28°45'42"N	17°53'26"W	2230	-6.55°	38.28°	30.388	23.987	38.714
VERITAS	31°41'18"N	110°53'00"W	1270	10.42°	58.27°	24.915	40.299	47.379
San Pedro Martir (Mexico)	31°02'00"N	115°25'00"W	2800	11.5°	56.07°	25.385	38.596	46.196
Sierra Negra (Mexico)	18°59'00"N	97°18'00"W	4000	4.75°	47.08°	27.768	29.868	40.782
Hanle (India)	32°45'36"N	78°57'36"E	4515	1.55°	50.47°	31.853	38.604	50.049
Oman A	23°6'00"N	57°31'5"E	2000	1.08°	35.37°	35.029	24.869	42.959

Table 2.1: Parameters of the candidate sites for the Cherenkov Telescope Array.

Chapter 3

Monte Carlo Simulations

In astro-particle physics Monte Carlo simulations are used to generate particle showers, hereafter referred to as events. These are then fed into the detector simulation. Hence, it is possible to design detectors and understand their performance as well as to compare their potential. To get accurate results, we need a lot of data [18, 19].

Events are generated using a random number generator. The programs use theoretical calculations of the processes under consideration and additional information e.g. information about the spectra of incident particles. Also the generation of Cherenkov light is taken into account. The simulation of photon showers gives an estimate on the detectable flux of the array. The performance of a telescope array of IACT like CTA depends on a large number of technical and design parameters. This chapter contains a summary of the most important simulation tools and parameters which were used during this study: CORSIKA and sim_telarray.

3.1 Simulation tools

3.1.1 Shower simulation: CORSIKA

CORSIKA [20] is a program used to simulate extensive air showers, EAS. These particle showers are initiated by high energy cosmic ray particles which can be e.g. protons, light nuclei up to $A \leq 56$ (iron) or photons. In our case it was a primary photon. The particles are tracked through the atmosphere, interact, annihilate or decay and produce secondary particles. The coordinate system of CORSIKA is defined as a Cartesian coordinate system as shown in Figure 3.1 [21]. The positive x-axis points to the magnetic north, the positive y-axis to the west and the z-axis upwards. The origin of the system is at sea level. The zenith angle Θ is measured between the direction of the EAS and the negative z-axis. The azimuth angle φ is defined as the angle between the positive x-axis and the horizontal component of the particle momentum vector and is counted counterclockwise. From a starting point which is at the upper border of the atmosphere (about 120 km a.s.l. in CORSIKA) the place of the first interaction is calculated. The height and the target nucleus of this interaction are selected randomly. At each observation level the coordinates of the first interaction point of each particle are set to $(0, 0, z_{obs})$.

The electromagnetic interactions are described by the interaction program EGS4 [22]. It delivers detailed information of all electromagnetic particles such as momentum, space coordinates or propagation time. This package treats annihilation, Bhabha scattering, bremsstrahlung, Møller scattering and multiple scattering for electrons and positrons. Gamma rays may undergo Compton scattering, pair production and photoelectric effect, depending on the energy of the particles. The deflection of charged particles in the geomagnetic field is calculated by an approximation which is only valid for small deflection angles. Low energy particles at high altitude may have significant path lengths and large deflection angles. The program EGS4 limits the deflection angle below $11.5°$ for each step. CORSIKA also simulates the Cherenkov light emission which is needed to characterize the candidate sites. The probability of electrons, positrons or gamma rays producing a charged particle at the next observation level is a function of their altitude and energy. Atmospheric absorption and scattering of Cherenkov light is also taken into account. Writing the origin height of each photon bunch onto the Cherenkov output, the absorption can be introduced later when analyzing the output data [23].

With the IACT option of CORSIKA we simulate the Cherenkov light hitting any arrays of telescopes. Each telescope can be represented using a sphere with a specific radius on the ground [24]. The Cherenkov light which passes through the sphere is stored and can be used then to a detailed detector simulation. The height of emission of each photon bunch is stored too. Each air shower was re-used

several times (in our simulations: 10 times) with random displacements because the CPU time of the simulation is relatively large. CORSIKA version 6.735 was used.
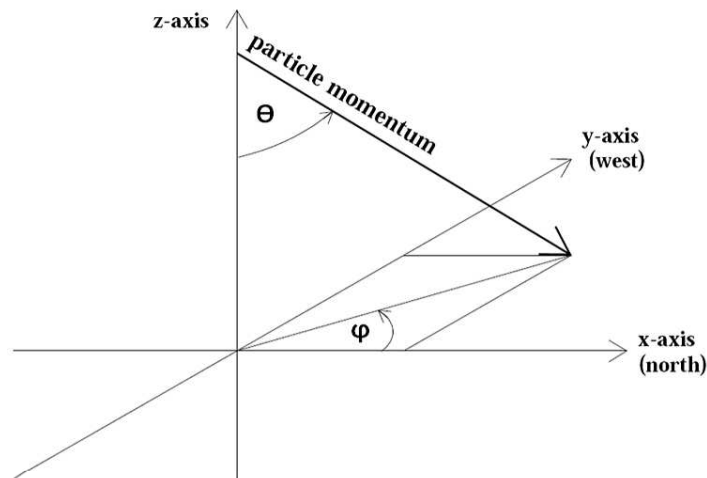
Figure 3.1: Coordinate system in CORSIKA [21].

3.1.2 Detector simulation: sim_telarray

The package sim_telarray was developed for H.E.S.S. and simulates the atmospheric impact on the Cherenkov light transport as well as the details of the detector response [25]. The detector simulation sim_telarray takes the Cherenkov photons from CORSIKA (with no intermediate storage on disk) and simulates the transport through the atmosphere and the reflection of the Cherenkov light in the telescope up to its detection within the cameras. The simulation package is very flexible and consequently, we can specify the entire detection process, starting from the reflector layout, optical ray-tracing of the photons until the recording of the signal by the cameras (including camera layout, the registration and digitization of the photon by the electrons of the photomultiplier tubes (PMT)) [24]. Here we used the benchmark array configuration with nine telescopes on a regular grid. The spacing between two neighboured telescopes is 80 m. Each telescope has a diameter of 23 m and an area of about 420 m^2 with a field-of-view of 5° and a pixel size of 0.09 deg given by the cameras [16].

3.2 Input parameters for simulations

In this subsection the Monte Carlo samples used for the simulations are presented. All in all we simulated γ-rays to get an estimation of the efficiency of the detection of sources for the different candidate sites. The primary particles come from different directions:

- Zenith angle Θ: 20° and 40°

- Azimuth angle φ:
  - → 0° - from north to south
  - → 90° - from east to west
  - → 180° - from south to north
  - → 270° - from west to east

3.2.1 Simulation of the geomagnetic field

We calculated the lateral distribution of Cherenkov photons using the geomagnetic field derived from the National Geographic Data Center [12] for each of the twelve candidate sites. For the calculation we

used CORSIKA without the simulation of telescopes and a primary γ-ray beam with a fixed energy of 100 GeV. This is the low energy limit where today's experiments can detect showers. We simulated a spectrum from 250 nm to 700 nm. Below a wavelength of 250 nm the absorption in the atmosphere and the spectral sensitivity of the PMT of the telescope cameras make the detection difficult. The Lorentz force is taken into account because the electrons and positrons which produce the Cherenkov photons are deflected in the geomagnetic field. The input parameters for the simulation of the geomagnetic field with CORSIKA are shown in Appendix A.

3.2.2 Simulation of Extensive Air Showers

For a given telescope configuration and arrangement of CTA, the energy threshold and effective detection area of primary γ-rays are determined by the lateral and angular distribution of the Cherenkov photons and the trigger conditions of the hardware. We chose two sites in the southern and two sites in the northern hemisphere as well as one reference site. The latter is Namibia with the observatory H.E.S.S. Extensive Air Showers and their detection with the telescope array were simulated for these sites with the help of CORSIKA and sim_telarray. The primary γ-rays are simulated with an E^{-2}-spectrum in the energy range from 3 GeV to 300 GeV. Using Monte Carlo simulations the detected energy spectra of the chosen sites are calculated for nine telescopes with a diameter of 23 m (FoV=5°, pixel size=0.09°), arranged on a regular grid. Cherenkov photons must be detected in at least two telescopes within a time window of 120 ns. A telescope triggers if there are at least three neighbored pixel with at least five photoelectrons in a time interval of 30 ns. This means that there should be at least 15 photoelectrons to trigger one telescope. For the simulations of the Extensive Air Showers we used the input parameters for CORSIKA and sim_telarray which are shown in the Appendix B.

Chapter 4

Influence of the geomagnetic field

The Earth's magnetic field deflects the electrons and positrons in the EAS. Therefore, the shape of the electromagnetic shower depends on the longitude and latitude of the location and the azimuth angle of the air shower. If we want to find the best site for the Cherenkov Telescope Array, we need to consider the influence of the geomagnetic field on the sensitivity of the telescopes.

4.1 Characterization of the geomagnetic field

At first, we want to characterize the geomagnetic field of each of the twelve candidate sites. The coordinate system which was used throughout this study is shown in Figure 4.1. For this simulation the optical axis of the telescope has always been set parallel to the direction of the primary particle which passes through the atmosphere until it reacts with the air nuclei.
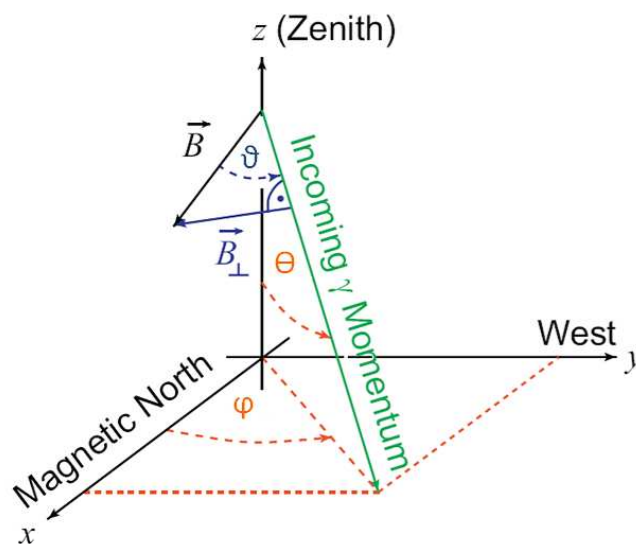
Figure 4.1: The definition of the coordinate system used throughout this work. The angle ϑ is measured between the direction of the EAS and the direction of the geomagnetic field [26], The zenith Θ and the azimuth angle φ describe the incoming gamma-ray.

Figures 4.2 - 4.5 show the absolute value of the component of the geomagnetic field strength $|\vec{B_\perp}|$ (in μT) normal to the direction of the Extensive Air Showers versus azimuth and zenith angle for the 12 candidate sites: ALMA and H.E.S.S. observatory, Salar de Pocitos, El Leoncito, La Silla, Beaufort West, La Palma, VERITAS, San Pedro Martir, Sierra Negra, Hanle and the site of Oman. The azimuth angle is defined like in the CORSIKA program [20] and refers to the momentum of the incoming gamma-ray. An azimuth angle of 0° means that the particle comes from the north and flies into the south direction, 180° describes the opposite situation. The figures used the measured total intensity of the geomagnetic field which we obtained from the epoch 2005 International Geomagnetic Reference Field (IGRF) model of the National Geographic Data Center [12]. The values are listed in Table 2.1.

For San Pedro Martir (Mexico), the minimum influence of the geomagnetic field is expected to occur

for EASs which develop in the direction of the magnetic north at a zenith angle:

$$\Theta = (90° - |I|) = (90° - 56.1°) = 33.9° \tag{4.1}$$

and an azimuth angle $\varphi = 0°$. At this point the angle between the shower axis and the Earth's magnetic field ϑ becomes zero (Table 4.1). As seen in Table 2.1, Mexico has an inclination of approximately 56.1°, thus the maximum influence is expected for EAS developing perpendicular to the direction of the lines of the geomagnetic field, for Mexico at $\Theta \approx 56.1°$ and $\varphi = 180°$. For Beaufort West in South Africa, the minimum influence of the Earth's magnetic field should occur at a zenith angle $\Theta \approx 24.6°$ and $\varphi = 180°$ and the maximum influence at $\Theta \approx 65.4°$ and $\varphi = 0°$ which can not be seen on the diagram because we simulated in the angular range of zenith from 0° to 60°. In this range telescope observing takes place [26].

Site	Inclination	Minimum influence		Maximum influence	
		Θ	φ	Θ	φ
ALMA	-20.2°	69.8°	180°	20.2°	0°
H.E.S.S.	-64.6°	25.4°	180°	64.6°	0°
Salar de Pocitos	-22.6°	67.4°	180°	22.6°	0°
El Leoncito	-31.8°	58.2°	180°	31.8°	0°
La Silla	-28.6°	61.4°	180°	28.6°	0°
Beaufort West	-65.4°	24.6°	180°	65.4°	0°
La Palma	38.3°	51.7°	0°	38.3°	180°
VERITAS	58.3°	31.7°	0°	58.3°	180°
San Pedro Martir	56.1°	33.9°	0°	56.1°	180°
Sierra Negra	47.1°	43.9°	0°	47.1°	180°
Hanle	50.5°	39.5°	0°	50.5°	180°
Oman A	35.4°	54.6°	0°	35.4°	180°

Table 4.1: Angle of the minimum influence and maximum influence of the geomagnetic field on the air shower development. For more details about the geomagnetic field see Table 2.1.

The geomagnetic field has the minimum influence in the southern hemisphere if the gamma-ray comes from the south ($\varphi = 180°$). In the northern hemisphere the situation is opposite.

ALMA 22°59'56''S, 67°45'39''W - Magnetic Field [μT]

H.E.S.S. 23°16'18''S, 16°30'00''E - Magnetic Field [μT]

Salar de Pocitos (Argentina) 24°26'40''S, 67°06'10''W - Magnetic Field [μT]
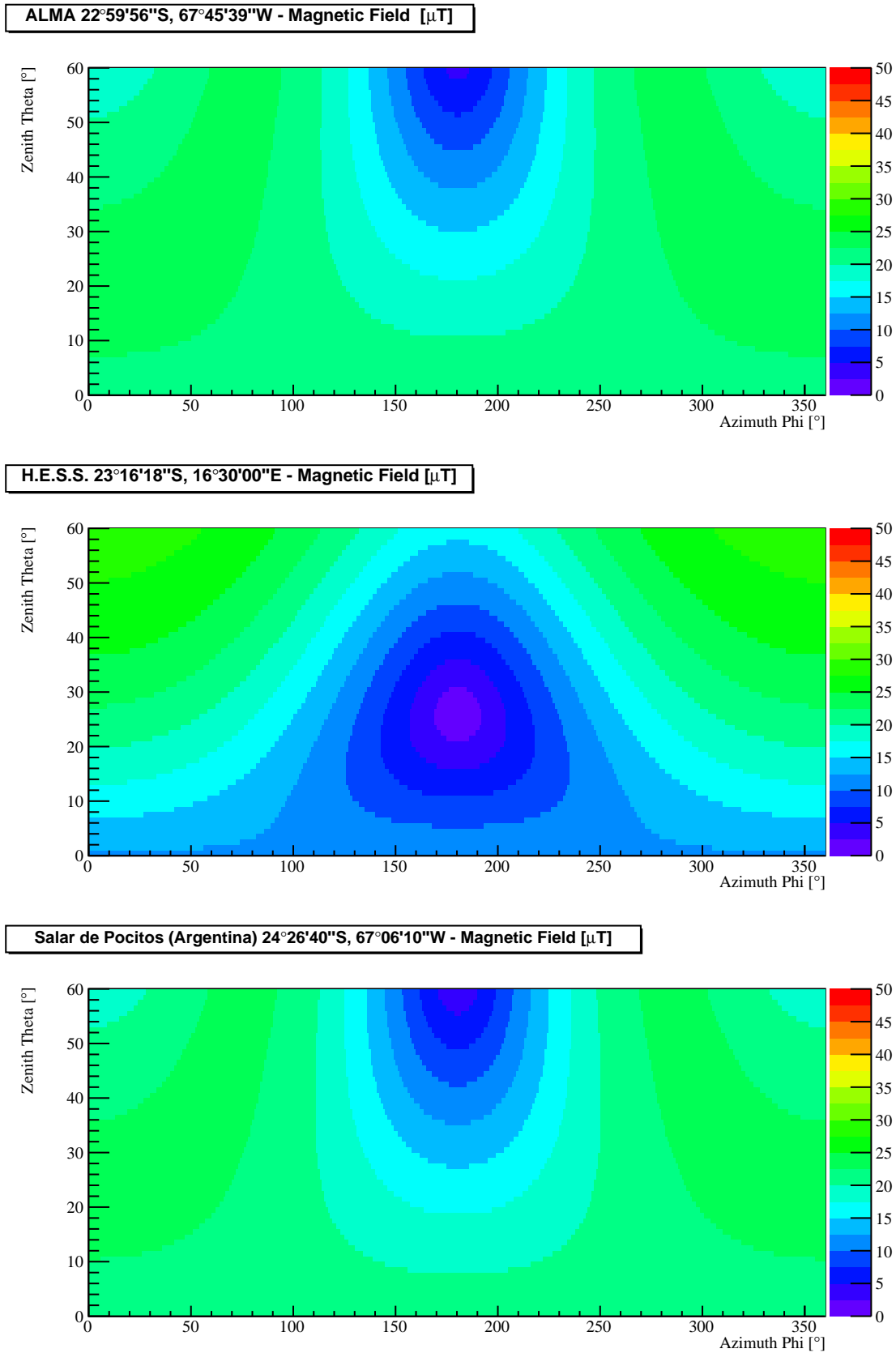
Figure 4.2: Absolute value of the component of the geomagnetic field strength versus the direction of the EAS at the site candidates the ALMA telescope, H.E.S.S. observatory and the site candidate for CTA Salar de Pocitos.
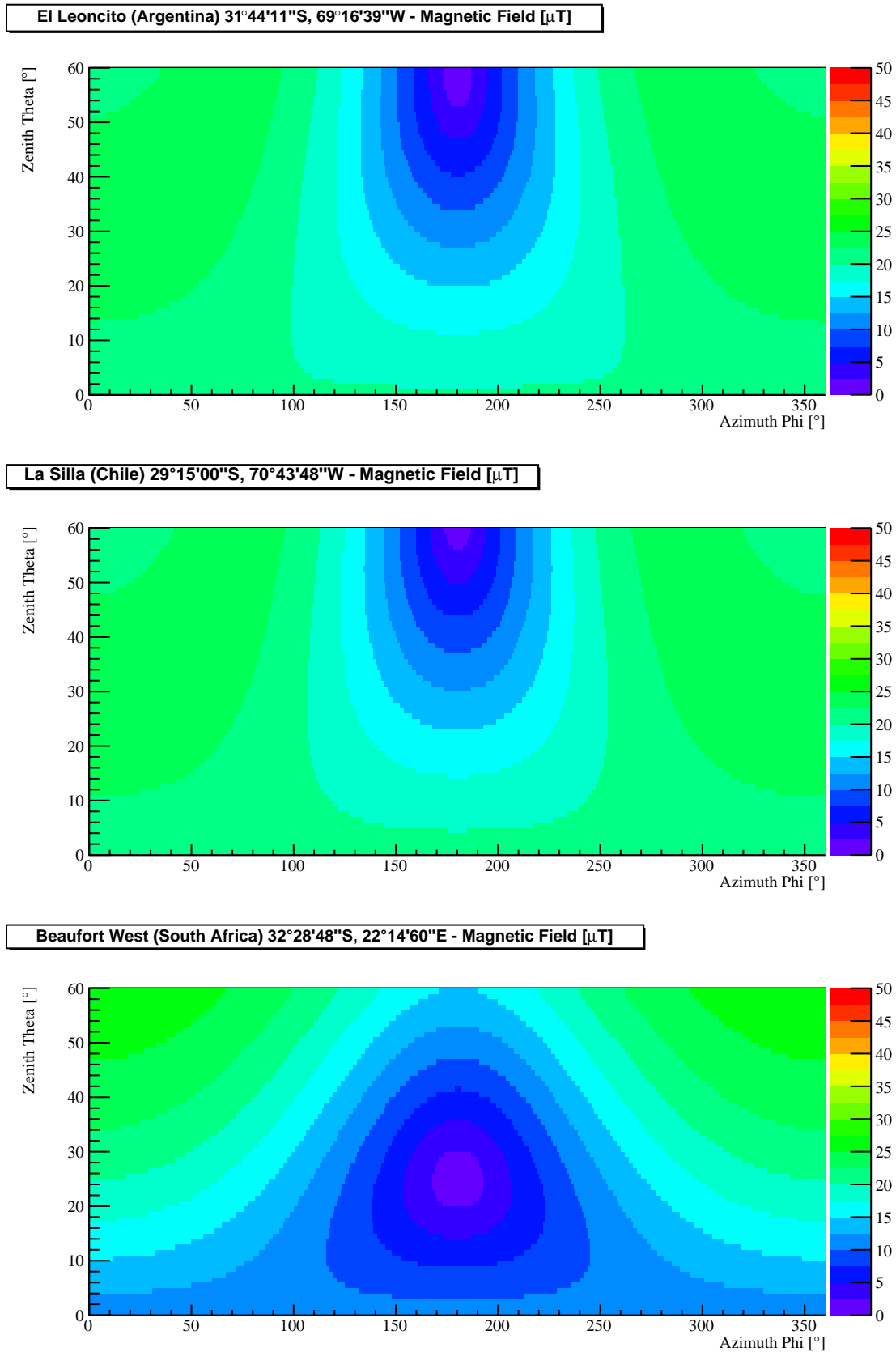
Figure 4.3: Absolute value of the component of the geomagnetic field strength versus the direction of the EAS at the site candidates for CTA El Leoncito, La Silla and Beaufort West.
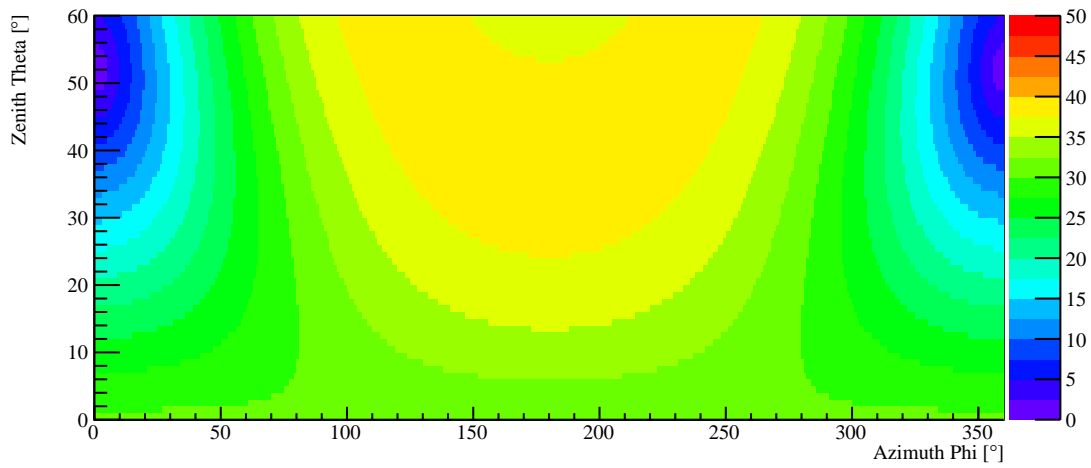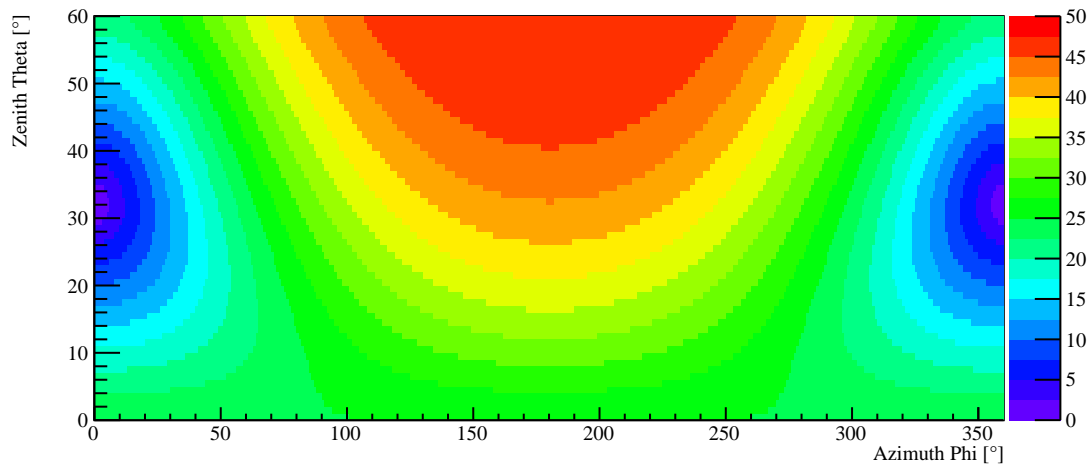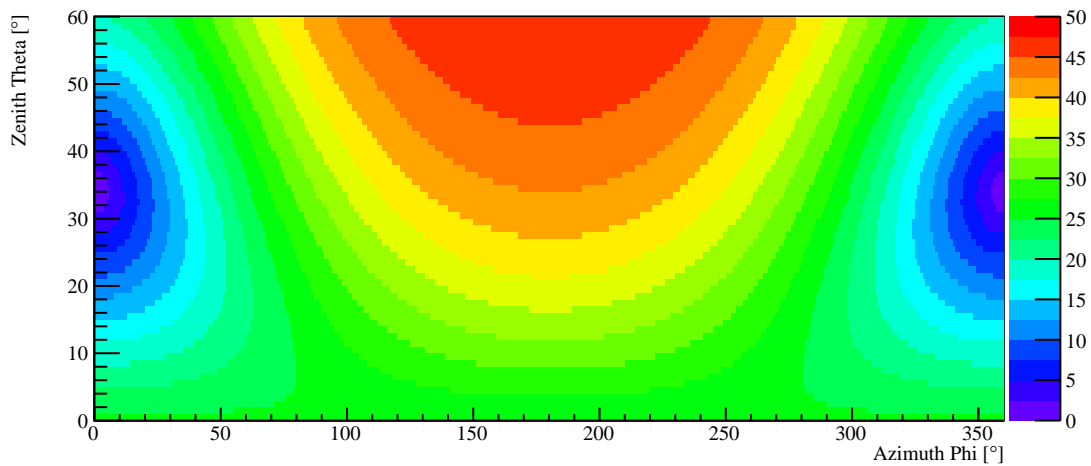
Figure 4.4: Absolute value of the component of the geomagnetic field strength versus the direction of the EAS at the site candidates the VERITAS observatory and the site candidate for CTA at La Palma and in San Pedro Martir.

Sierra Negra (Mexico) 18°59'00"N, 97°18'00"W - Magnetic Field [μT]

Hanle (India) 32°45'36"N, 78°57'36"E - Magnetic Field [μT]

Oman A 23°6'00"N, 57°31'5"E - Magnetic Field [μT]
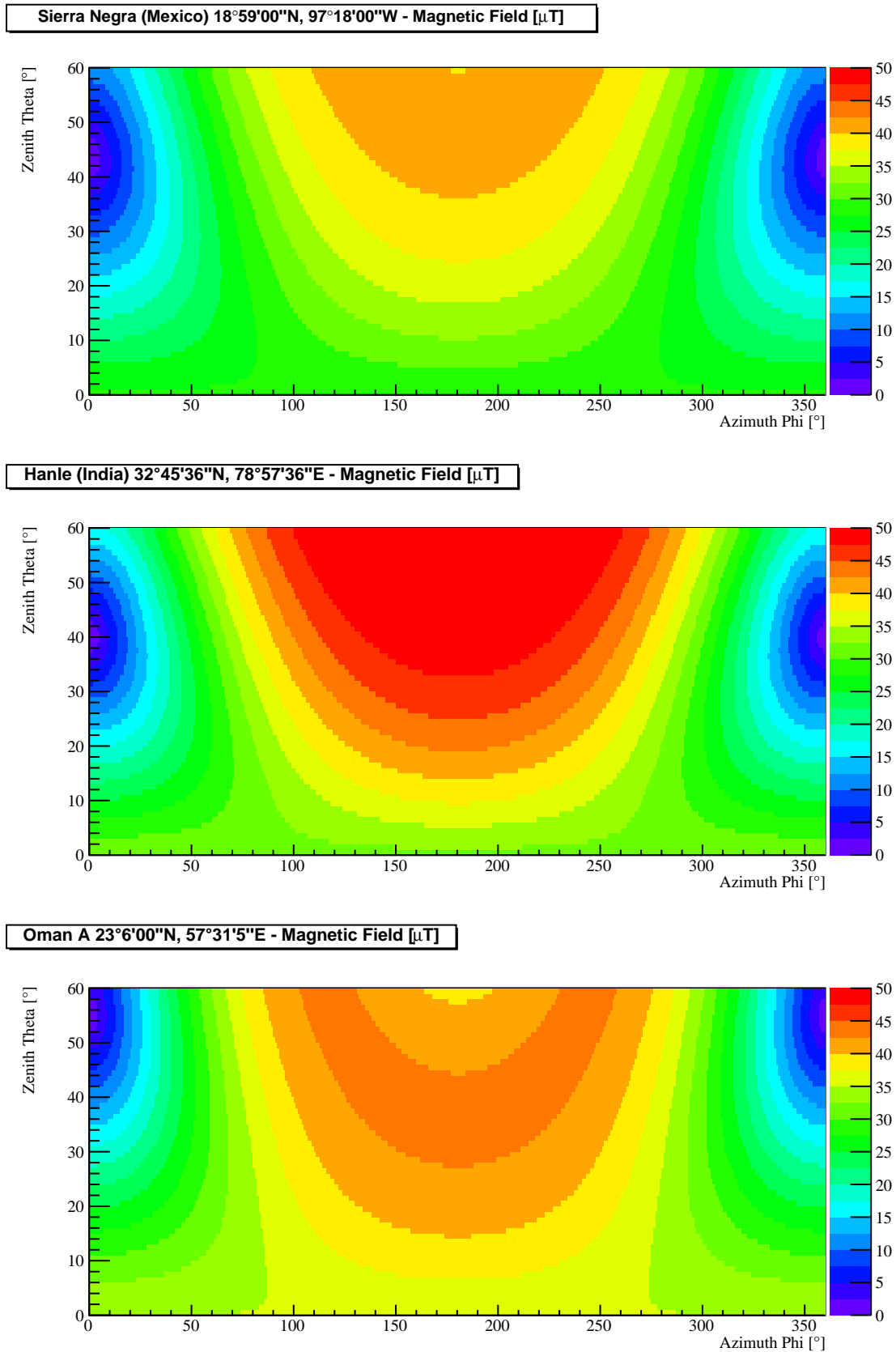
Figure 4.5: Absolute value of the component of the geomagnetic field strength versus the direction of the EAS at the site candidates for CTA Sierra Negra, Hanle and Oman.

4.2 Cherenkov photon density

To compare the sensitivities of the sites, we simulate the lateral distribution of the particle showers for each of the 12 candidate sites and the reference site without geomagnetic field, $B = 0$. Each site is set at an altitude of 2000 m as well as their specific height. For the influence of the geomagnetic field on the particles we use the parameters of the field which are given in Table 2.1. The lateral distribution which is influenced by the Cherenkov angle and Coulomb scattering angle shows the density of Cherenkov photons on the ground as a function of the impact parameters such as the energy of the primary particle and the direction where the particles come from. We simulate for various azimuth e.g. 0°, 90°, 180° and 270° and zenith angles at 20° and 40°. The energy of the primary photon is 100 GeV. Firstly, the altitude of all sites is 2000 m because we want to simulate only the geomagnetic effects on the showers. If we would simulate at the specific heights, we would simulate both the shower development and the geomagnetic effects. This is important for a comparison between the sites.

4.2.1 Cherenkov light characteristics

The lateral distributions of Cherenkov light originating from simulated γ-ray air showers at the site of Beaufort West at a zenith angle of 20° (left-hand site) and 40° (right-hand site) are shown in Figure 4.6. The respective graphs of the other locations are shown in Appendix C and D. The error bars show indicate statistical errors only [27]. The input parameters of these simulations are given in Appendix A. The distribution has a very characteristic shape which is constant to a rim at about 130 m, the lightpool. Beyond the rim the light intensity falls rapidly because the Cherenkov angle Θ_C changes with the refraction index n which is a function of height. The shape is nearly independent of the energy of the primary photon [28, 29]. For the following discussion, just the Cherenkov photons in the lightpool are important.

(a) $\Theta = 20°$, 2000 m   (b) $\Theta = 40°$, 2000 m

(c) $\Theta = 20°$, 1800 m   (d) $\Theta = 40°$, 1800 m
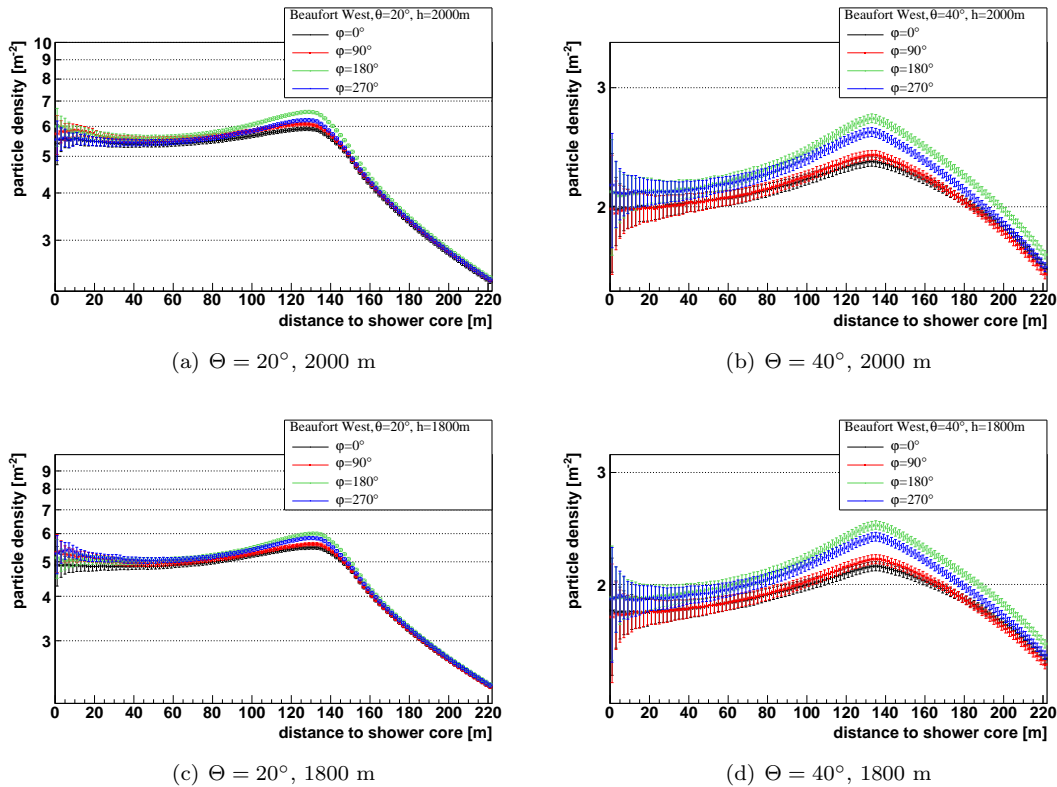
Figure 4.6: Lateral distribution of the density of 250-700 nm Cherenkov photons in simulations of 100 GeV gamma-rays for the site of Beaufort West for zenith angles Θ at 20° and 40°, azimuth angles φ at 0°, 90°, 180° and 270° and altitudes of 2000 m (top) and 1800 m (bottom).

Appendix C shows the lateral distribution of Cherenkov photons on the ground at an altitude of 2000 m for each site. For these computations, we have an amount of Cherenkov photons of approximately $3 \cdot 10^9$ for a zenith angle of $20°$ and about $2 \cdot 10^9$ at $40°$. The particle density is approximately 5 to 6 Cherenkov photons/m^2 at $20°$ and about 2 photons/m^2 for $40°$ because the path length through the atmosphere is longer for larger incidence angle of the primary photon. As a consequent, more particles are absorbed from the air molecules through the travel in the atmosphere.

In the southern hemisphere the density of Cherenkov photons is largest if the observation takes place at an azimuth angle of $180°$, where the primary gamma-ray comes from the south and flies into the north, and smallest at $0°$. If we compare the density inside the lightpool of the sites, there are almost no variations between the H.E.S.S. site and Beaufort West because the influence of the geomagnetic field is nearly the same. At the site of Beaufort West the variation in Cherenkov photons/m^2 inside the lightpool is from about 6% to about 17% at $\Theta = 20°$ and from about 13% to about 17% predicted at $\Theta = 40°$. This is in accordance to the influence of the geomagnetic field on the shower development. The site of El Leoncito shows a similar behaviour, the particle density varies from about 5% to about 22% at $\Theta = 20°$ and from about 11% to about 22% at $\Theta = 40°$. A comparsion of the density of light between Beaufort West and El Leoncito follows that the density of Cherenkov photons increases slightly at the site of Beaufort West.

In the northern hemisphere the density of Cherenkov photons is smallest if the primary gamma-ray comes from the south direction. If it flies from the north to the south, the density is largest. At the location of the Canary Island La Palma, the variation in particle density is from about 8% to about 16% at $\Theta = 20°$ and from about 16% to about 8% predicted at $\Theta = 40°$. The difference at San Pedro Martir is a bit larger. It is from about 12% to about 24% at $\Theta = 20°$ and from about 19% to about 47% at $\Theta = 40°$. A comparison between both sites at a zenith angle of $20°$ and an azimuth of $0°$ shows that the density of Cherenkov photons increases at the site of San Pedro Martir. Predictions at $\Theta = 40°$ indicates the opposite situation. The reason is the absolute value of the component of the geomagnetic field strength versus to the direction of the EAS (see Figure 4.4). At an azimuth of $180°$ La Palma shows the higher density which is in accordance with the geomagnetic field strength. For a decision, the results at $\varphi = 90°$ and $\varphi = 270°$ are important. Especially at $\Theta = 40°$ it is seen that the number of Cherenkov photons/m^2 increases slightly at La Palma.

Consequently, the minimum influence of the geomagnetic field on the shower development is at the sites of Beaufort West and La Palma. It is also important to see that the geomagnetic field has a larger influence on the shower development on the locations in the northern hemisphere because the differences in particle density predicted at an azimuth angle of $0°$ and $180°$ are larger than for the locations in the southern hemisphere. This is in accordance to the characterization of the geomagnetic field which was described in the previous chapter.

If we look at the results obtained at the real altitudes of all candidate sites of CTA (Figure 4.6 and Appendix D), it is obvious that there are much more photons/m^2 for locations at higher altitudes like El Leoncito (2500 m) and San Pedro Martir (3000 m) than for locations at lower ones like Beaufort West (1800 m) and La Palma (2200 m). In comparison to about 7 Cherenkov photons/m^2 at El Leoncito, there are about 5 Cherenkov photons/m^2 at the site of Beaufort West at $\Theta = 20°$. Furthermore, there are about 10 Cherenkov photons/m^2 at San Pedro Martir and only about 6 photons/m^2 at La Palma at $\Theta = 20°$ which is a difference of about 30% to 40%. At a zenith angle of $40°$ the density of Cherenkov photons is on the order of 20% to 30% higher at the site of San Pedro Martir. These results originate from the fact that at altitudes of e.g. 3000 m there are more particles in the shower than at altitudes of 2200 m because the intensity of light is the integral over the number of particles in the shower and there are more particles at higher elevations than at lower ones. This implies that the choice of very high altitudes for the operation of CTA would allow a significant reduction of the energy threshold which is described in Section 4.3 and a higher density of Cherenkov photons on the ground.

From the point of the geomagnetic field the best location would be Beaufort West in the southern hemisphere and La Palma in the northern hemisphere. There are the smallest influence of the geomagnetic field respectively in each hemisphere. The disadvantages in Cherenkov photon density which arise from a larger influence of the geomagnetic field are compensated by a higher altitude of the locations and vice versa. Looking at the real altitudes, El Leoncito in Argentina and San Pedro Martir in Mexico have larger densities of Cherenkov photons on the ground than the other sites.

4.2.2 Comparison of lateral distribution to B=0

Appendix E shows the lateral distribution of Cherenkov radiation from air showers induced by γ-rays of an energy of 100 GeV for all sites and for a comparison to a site with $B = 0$ at an altitude of 2000 m. Firstly, within a radius of about 130 m from the shower core the density of Cherenkov photons on the ground has a rather flat distribution and hits the lowest point at 130 m. The graphs reveal differences between northern and southern locations. For example, if we look at the predictions obtained at a zenith angle of 20° and an azimuth of 0°, the locations in the northern hemisphere indicate smaller variations in comparison to the site with $B = 0$, especially at low distances to the shower core. The differences in the photon density on the ground are from about 1% to about 7% in the northern hemisphere and from about 4% to about 13% in the southern hemisphere. Otherwise at an azimuth of 180° the graphs show the opposite situation. The southern places almost agree with the $B = 0$ site. There are about 1% to 10% less Cherenkov photons/m^2 inside the lightpool for locations in the southern hemisphere than for a location with $B = 0$. The Cherenkov photon density of the northern sites is about 10% to 25% smaller. It accords with the results which were obtained in previous chapters. The influence of the geomagnetic field on the shower development is smallest and the sensitivity is greatest at an azimuth angle of 180° in the southern hemisphere and at 0° in the northern hemisphere because there are more Cherenkov photons on the ground.

4.2.3 CTA site selection

CTA will have two telescope arrays, one in the southern hemisphere and the other one in the northern hemisphere. It is not recommended to choose a site which is located higher than 4000 m because the optimum overall performance is obtained for site altitudes between 1500 and 4000 m [16]. It is also important that there are reasonable flat areas of about 1 km^2 (north) and 10 km^2 (south) for the large number of Cherenkov telescopes. At higher altitudes it will be difficult to find a big flat area. Therefore, we chose two sites in the south and two in the north for the following simulations. By comparing the lateral distributions from all sites, the places of Beaufort West in South Africa and El Leoncito in Argentina are similar to a fictitious site with $B = 0$. Both sites have a small total intensity of the geomagnetic field, ≈ 26 μT at Beaufort West and ≈ 24 μT at El Leoncito. In the northern hemisphere the sites La Palma and San Pedro Martir are similar to $B = 0$. They also have a small total intensity of the geomagnetic field compared to the other northern locations, ≈ 39 μT at La Palma and ≈ 46 μT at San Pedro Martir. From the point of the geomagnetic field and the Cherenkov light characteristics these four places are the best ones for the Cherenkov Telescope Array.
On the other hand there are several other facts which have to be considered, e.g. the energy threshold and the effective area. These will be discussed in the following chapters for the sites listed below:

- Beaufort West (South Africa)

- El Leoncito (Argentina)

- San Pedro Martir (Mexico)

- La Palma (Canary Island)

- H.E.S.S. (Namibia) to compare to an used site

4.2.4 Distribution of the position of Cherenkov photons

The density distribution of Cherenkov photons on the ground is shown in Figure 4.7 and 4.8. The shape of areas with equal density are ellipses. It is in accordance to the diagrams which were obtained from the lateral distribution. The red corresponds to the maximum Cherenkov photon density at a radius of about 130 m for a zenith angle of 20°. Inside this ring, the rim, the density is higher than beyond. There are considerably less photons on the ground for electromagnetic showers at a zenith angle of 40°. The semi-major axis becomes longer and the semi-minor axis shorter. More Cherenkov photons get absorbed in the atmosphere since the distance to ground is larger.
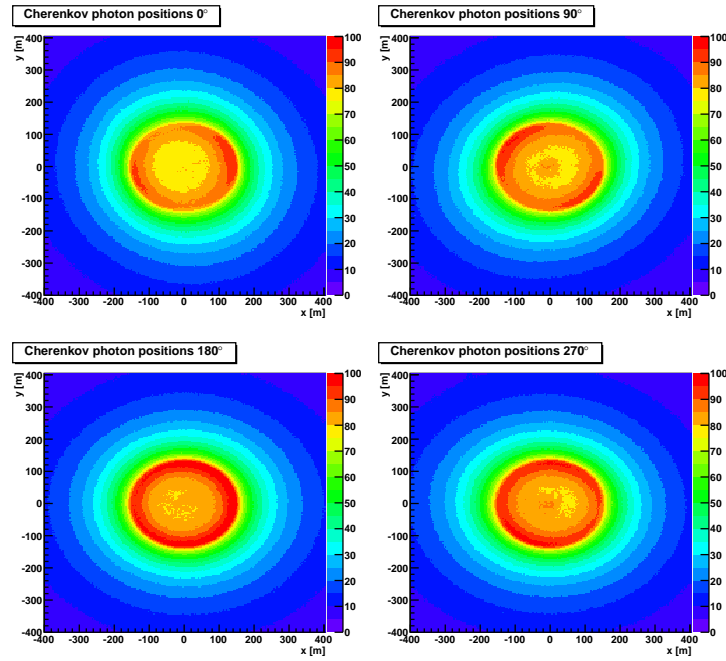
Figure 4.7: Cherenkov photon density distribution on the ground (in photons/m^2) for the Beaufort West site for a zenith angle $\Theta = 20°$ and azimuth angles φ at $0°$, $90°$, $180°$ and $270°$.
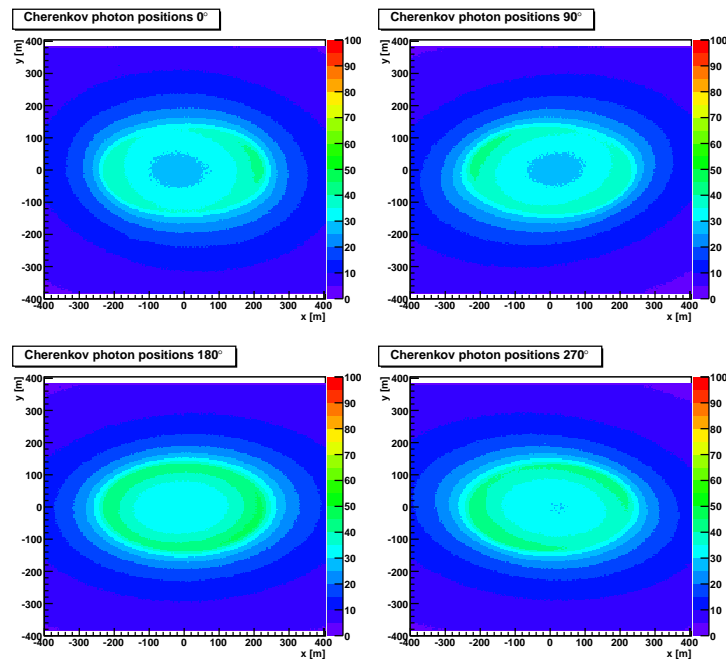
Figure 4.8: Cherenkov photon density distribution on the ground (in photons/m^2) for the Beaufort West site for a zenith angle $\Theta = 40°$ and azimuth angles φ at $0°$, $90°$, $180°$ and $270°$.

4.3 Photon energy spectra

The first experiment in the observation of high energy photons which had a great success was the Fred Lawrence Whipple Observatory in Southern Arizona in the United States. It achieved an energy threshold of approximately 350 GeV. The new generation of Cherenkov telescopes has the aim to reduce the energy threshold to below 100 GeV. The crucial quantity here is the number of Cherenkov photons which are collected. With a reduction in the energy threshold of ground-based instruments, it is expected to increase the number of extragalactic objects visible in high energy gamma rays. The energy threshold depends on the atmospheric depth above the detector, the ratio of the collection area (size of detector) to the enclosed area A_0 and the ability to detect different components of an EAS [10]. The energy threshold will be estimated in the following chapter for selected sites. The first significant improvement in sensitivity and energy resolution of the IACT technique was achieved in the last generation of instruments by HEGRA. This experiment used the stereoscopy, where particle showers are imaged simultaneously by several telescopes. All currently operated observatories such as H.E.S.S., VERITAS, MAGIC and CANGAROO-III using a stereoscopic shower reconstruction. The multiple view with more than one telescope allows far more precise measurements of the shower parameters like energy and direction of the origin of cosmic ray as well as a better background suppression [30]. CTA has the aim to lower the energy threshold to below 100 GeV.

4.3.1 Energy threshold

Using Monte Carlo simulations the generated and reconstructed photon spectra are estimated for an array of nine telescopes placed at Beaufort West, H.E.S.S., El Leoncito, La Palma and San Pedro Martir. The input parameters for the generation of events using CORSIKA are listed in the Appendix B. The primary γ-rays are simulated with an E^{-2}-spectrum in the energy range from 3 GeV to 300 GeV. The system consisting of nine telescopes is installed at the specific altitude of each site and at the fictitious height of 2000 m. They are arranged on a regular grid with a linear size of 80 m. Each telescope has an aperture of 490 m^2 and is equipped with a camera of individual pixel size 0.09° and an effective FoV=5°. Events which are triggered in at least two telescopes within a time window of 120 ns will be considered for the study. The generated and the reconstructed number of Cherenkov photons per unit area per unit time as a function of the primary energy is shown in Figure 4.9 for the site of Beaufort West.

The energy spectra rise rapidly at low energies and reach a maximum at a certain energy, defining the energy threshold E_T. Below this energy there are still registered photons which can be detected when the primary gamma-ray penetrates deeply into the atmosphere before it undergoes interaction e.g. pair production and bremsstrahlung. Above the energy threshold, the flux of particles drops down. Above E_T, most of the particle showers are detected and the reconstructed energy spectrum approaches the generated input spectrum (grey line) which is the power-law spectrum of E^{-2}. At large primary energies the difference between the simulated and accepted spectra results from the fact that the active detection area A_0 which has a radius of 500 m and an area of about $8 \cdot 10^5$ m^2 is significantly larger than the physical size of the detector which has an area of about 3700 m^2. At low energies there are insufficient Cherenkov photons to trigger in at least two telescopes. Particle showers which reach the ground at the border of the detection area will not be registered in the detector since they are outside of the lightpool.

(a) $\Theta = 20°$, 2000 m

(b) $\Theta = 40°$, 2000 m
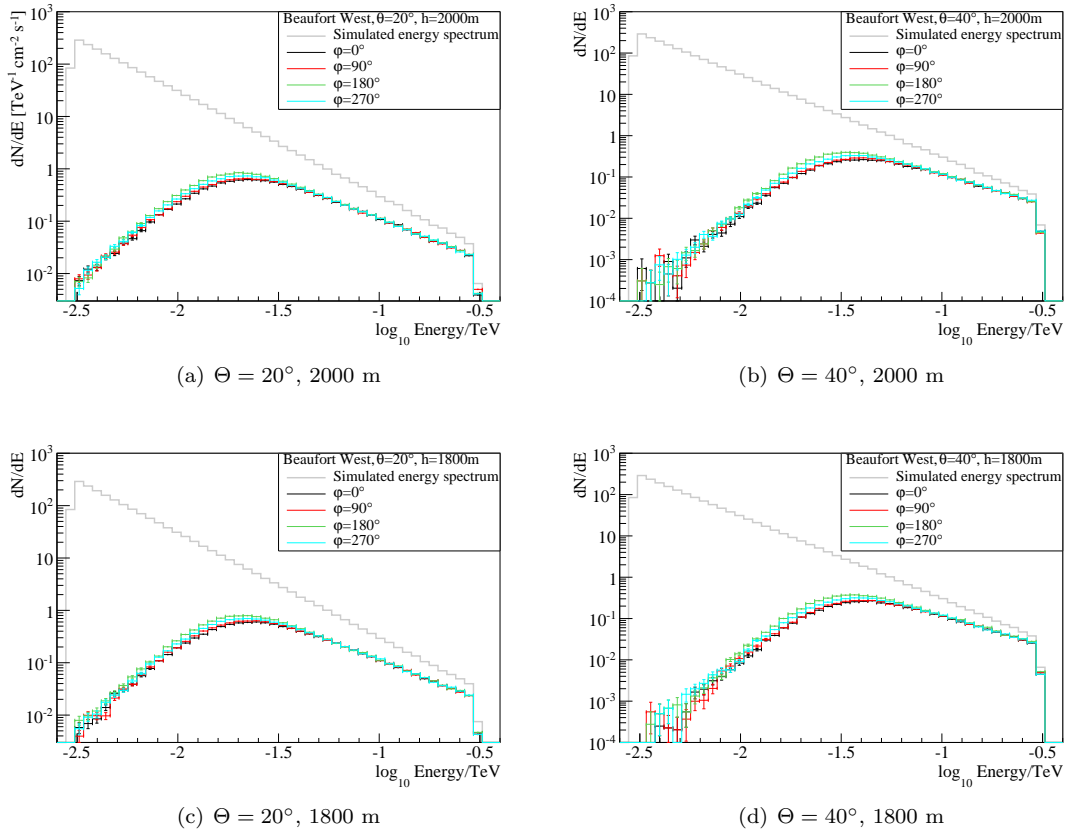
(c) $\Theta = 20°$, 1800 m

(d) $\Theta = 40°$, 1800 m

Figure 4.9: Energy spectra of the generated and reconstructed photons at Beaufort West versus energy for zenith angles Θ at 20° and 40°, azimuth angles φ at 0°, 90°, 180° and 270° and altitudes of 2000 m (top) and 1800 m (bottom).

The energy threshold of a Cherenkov telescope is a way to compare the response to a given source at different locations [29]. The comparison of the southern sites, Beaufort West and H.E.S.S. (Figure 4.10(a) and 4.10(b)), demonstrates that there are almost no variations in the photon energy spectra detected at an elevation of 2000 m. They show almost the same behaviour because the distance between H.E.S.S. and Beaufort West, and therefore the impact and the field intensity of the geomagnetic field between the locations is very small. Looking at Beaufort West and El Leoncito (Figure 4.10(c) and 4.10(d)), the differences are larger. Especially at low energies (3-5 GeV) Beaufort West has a better acceptance than El Leoncito; the number of particles per energy is higher at the site of Beaufort West. The graphs of La Palma and San Pedro Martir (Figure 4.10(e) and 4.10(f)) are quite similar but especially at low energies the energy spectra of the reconstructed photons of San Pedro Martir lies a little bit higher than the spectra of La Palma. These results agree well with the expectation from the absolute value of the vertical component of the geomagnetic field strength. At an azimuth angle of 0° and a zenith of 20° and 40° the absolute value of the vertical component is smaller at the site of San Pedro Martir. At an azimuth of 180° La Palma shows the slightly larger acceptance, especially at $\Theta = 40°$ which is in accordance with the expected impact of the geomagnetic field strength. To summarize, the fraction of detected photons is largest at an azimuth angle of 180° in the southern and at 0° in the northern hemisphere.
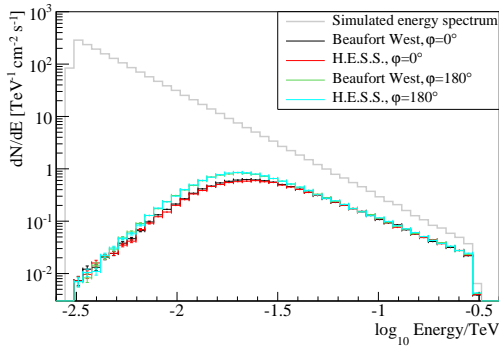
(a) Beaufort West and H.E.S.S. at $\Theta = 20°$
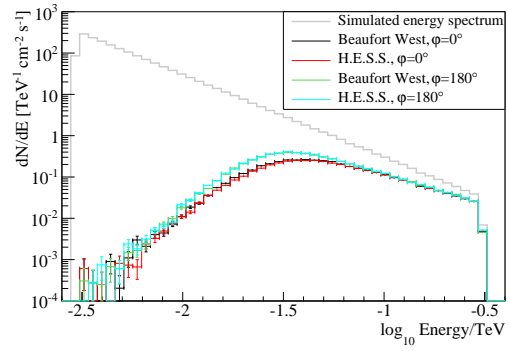
(b) Beaufort West and H.E.S.S. at $\Theta = 40°$
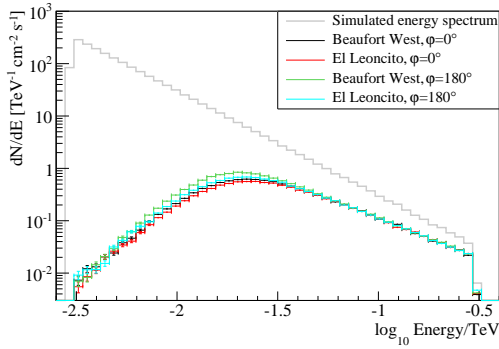
(c) Beaufort West and El Leoncito at $\Theta = 20°$
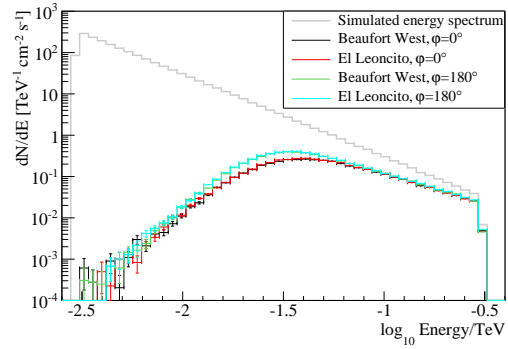
(d) Beaufort West and El Leoncito at $\Theta = 40°$
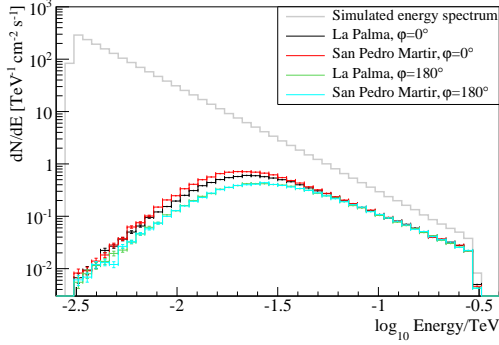
(e) La Palma and San Pedro Martir at $\Theta = 20°$
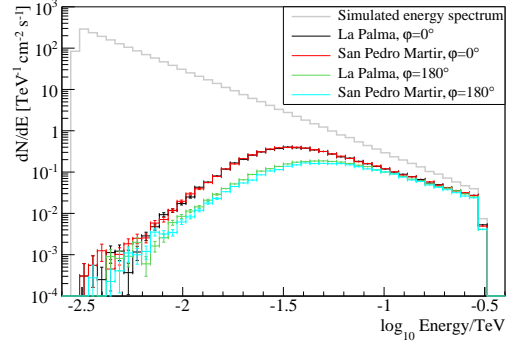
(f) La Palma and San Pedro Martir at $\Theta = 40°$

Figure 4.10: Comparison of the energy spectra of the reconstructed photons at Beaufort West and H.E.S.S.; Beaufort West and El Leoncito; La Palma and San Pedro Martir for zenith angles Θ at $20°$ and $40°$ and azimuth angles φ at $0°$ and $180°$ at an altitude of 2000 m.

The values of the energy threshold are listed in Table 4.2.

Site	Altitude h	Zenith $Theta$	Azimuth φ	E_T	A_{eff}
	[m]	[°]	[°]	[GeV]	[1000 m^2]
H.E.S.S	2000	20	0	25	100.1
	2000	20	180	20	87.3
Beaufort West	2000	20	0	22	81.5
	2000	20	180	20	85.2
El Leoncito	2000	20	0	25	91.7
	2000	20	180	22	87.3
La Palma	2000	20	0	22	78.1
	2000	20	180	25	69.9
San Pedro Martir	2000	20	0	20	75.8
	2000	20	180	27	82.0
H.E.S.S	2000	40	0	37	91.5
	2000	40	180	33	110.4
Beaufort West	2000	40	0	41	117.2
	2000	40	180	33	110.8
El Leoncito	2000	40	0	41	118.8
	2000	40	180	37	135.5
La Palma	2000	40	0	33	111.4
	2000	40	180	50	119.7
San Pedro Martir	2000	40	0	37	135.5
	2000	40	180	41	75.6
H.E.S.S	1800	20	0	25	92.0
	1800	20	180	20	84.1
Beaufort West	1800	20	0	25	94.9
	1800	20	180	22	100.3
El Leoncito	2500	20	0	22	81.8
	2500	20	180	20	78.5
La Palma	2200	20	0	22	80.9
	2200	20	180	27	85.8
San Pedro Martir	3000	20	0	20	60.0
	3000	20	180	18	61.7
H.E.S.S	1800	40	0	37	89.4
	1800	40	180	37	130.1
Beaufort West	1800	40	0	45	134.3
	1800	40	180	37	128.4
El Leoncito	2500	40	0	41	127.6
	2500	40	180	33	127.0
La Palma	2200	40	0	33	115.5
	2200	40	180	45	106.7
San Pedro Martir	3000	40	0	37	80.9
	3000	40	180	30	74.4

Table 4.2: Energy threshold E_T and effective detection area A_{eff} at a fictitious altitude of 2000 m and real altitudes.

All in all, San Pedro Martir in the northern hemisphere, the H.E.S.S. site and Beaufort West in the southern hemisphere have the smaller energy thresholds. The energy threshold is larger at larger zenith angles, the same applies to the effective detection area. The charged particles travel further through the atmosphere; consequently more particles are absorbed in the atmosphere; less Cherenkov photons reach the ground [31].

As energy threshold, the energy bin with the maximum content of flux is used. Fitting the curve to energy spectra results in an error of the position of the maximum. The values of the energy threshold and its error are given in Table 4.3.

Altitude	Zenith Θ	Azimuth φ	Position of the energy bin	Difference
[m]	[°]	[°]	[log_{10}Energy TeV]	
2000	20	0	-1.6 ± 0.6	39.1%
2000	40	0	-1.4 ± 0.3	22.3%
real altitude	20	0	-1.6 ± 0.7	41.2%
real altitude	40	0	-1.4 ± 0.4	28.5%

Table 4.3: The threshold energy E_T determined from a fit to the reconstructed energy spectrum and its error.

4.3.2 Effective detection area

In order to compare the photon detection sensitivity of the candidate sites, we need the effective detection area on the ground over which the detected showers are distributed. The effective detection area A_{eff} indicates the fraction of triggered showers. The larger the area, especially at low energies, the higher the sensitivity and efficiency of the candidate sites. The effective detection area at an energy E is given by:

$$A_{eff}(E) = \frac{N_{triggered}}{N_{simulated}} \cdot A_0, \qquad (4.2)$$

whereby $N_{simulated}$ is the number of simulated γ-ray showers which fall at random positions over a sufficiently large area A_0 and $N_{triggered}$ the number of showers which are triggered by the telescope and pass the selection criteria. For the aim of this work, a radius of 500 m is adequate for the calculation of A_0 [1] because inside this radius most of the Cherenkov photons are detected:

$$A_0 = \pi r^2 \approx 8 \cdot 10^5 \ m^2. \qquad (4.3)$$

Each bin content of the simulated energy spectra histogram was divided by the corresponding bin content of the triggered energy spectra. The resulting distributions for Beaufort West are shown in Figure 4.11 as well as in Appendix H and I for the other four sites. At low energies the ratio rises rapidly and reaches a plateau at high energies. The effective detection area of the locations is significantly larger than the physical size of the detector, about 3700 m^2, and goes to zero at small energies. Here particle showers do not produce enough Cherenkov light to trigger the telescopes. The Cherenkov light intensity is related to the energy of the primary photon and the distance to the shower core [29]. Looking at a zenith angle of 20° the effective detection areas at low energies are larger than for a zenith angle of 40° because more Cherenkov photons reach the ground.

---

[1]The radius is described with the argument CSCAT in Appendix B.

(a) $\Theta = 20°$, 2000 m

(b) $\Theta = 40°$, 2000 m
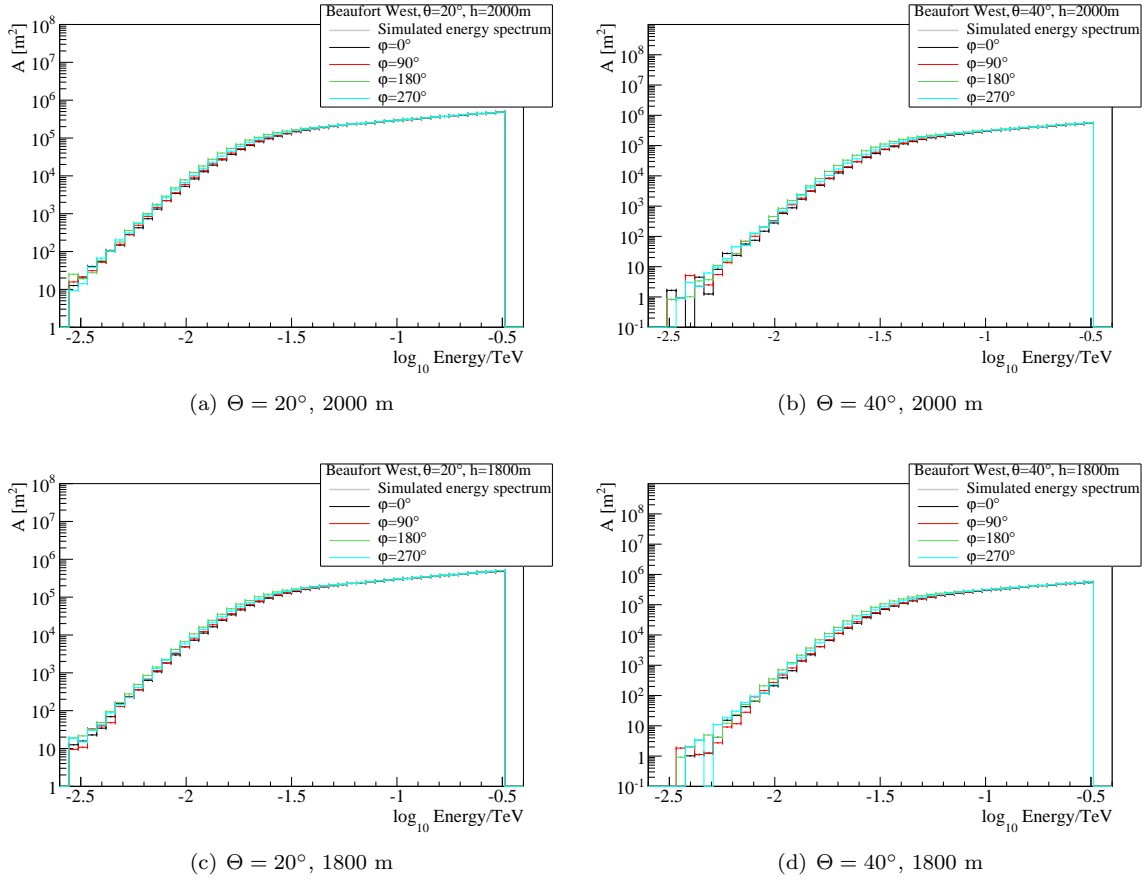
(c) $\Theta = 20°$, 1800 m

(d) $\Theta = 40°$, 1800 m

Figure 4.11: Effective detection area of Beaufort West versus energy for zenith angles Θ at 20° and 40°, azimuth angles φ at 0°, 90°, 180° and 270° and altitudes of 2000 m (top) and 1800 m (bottom).

In the region of the energy threshold, the area which is estimated from the simulations is highly dependent on the trigger criteria. The effective detection area of the sites in the southern hemisphere are largest at $\varphi = 180°$ and smallest at $\varphi = 0°$. The sites on the northern part of the Earth demonstrate the opposite behaviour because the influence of the geomagnetic field is opposite between northern and southern hemisphere. Table 4.2 lists the effective detection areas of the candidate sites calculated at the energy threshold E_T. The effective detection area depends on the zenith, the azimuth and on E_T. The table also shows that the effective detection areas of the locations in the southern hemisphere at $\varphi = 180°$ are not always larger than those ones at $\varphi = 0°$. The same applies to the location in the northern hemisphere. The fit of the energy spectra result in an error of the position of the energy threshold(Table 4.3). Using this error we can estimate the corresponding variation of the effective detection area. With 68.3% probability the correct value of the effective detection area is within a range of $\sigma = \pm 20 \cdot 10^3 \ m^2$.

(a) $\Theta = 20°$ (b) $\Theta = 40°$
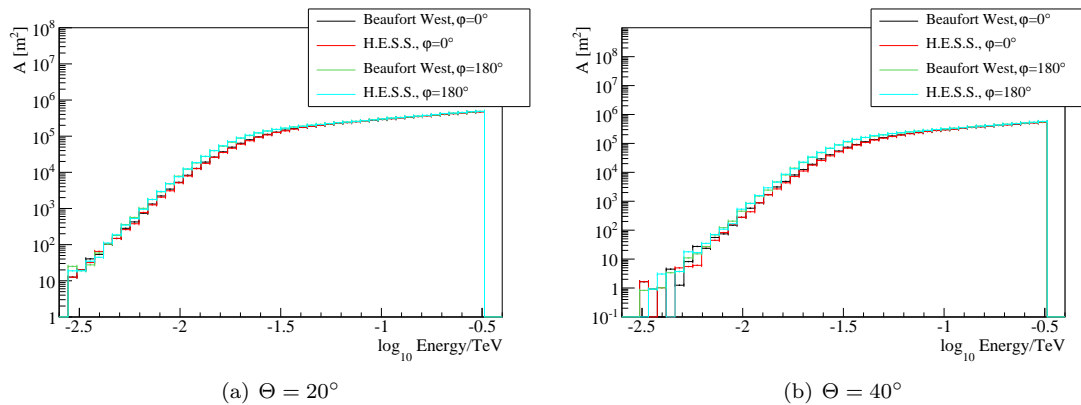
Figure 4.12: Comparison of the effective detection area at Beaufort West and H.E.S.S. at an altitude of 2000 m for azimuth angles φ at $0°$ and $180°$.

Site	Altitude h	Zenith Θ	Azimuth φ	E_T	A_{eff}	ΔA_{eff}
	[m]	[°]	[°]	[GeV]	[1000 m^2]	
H.E.S.S.	2000	20	0	25	100.1	22.8%
Beaufort West	2000	20	0	22	81.5	
H.E.S.S.	2000	20	180	20	87.3	2.5%
Beaufort West	2000	20	180	20	85.2	
H.E.S.S.	2000	40	0	37	91.5	-21.9%
Beaufort West	2000	40	0	41	117.2	
H.E.S.S.	2000	40	180	33	110.4	-0.4%
Beaufort West	2000	40	180	33	110.8	
H.E.S.S.	1800	20	0	25	92.0	-3.1%
Beaufort West	1800	20	0	25	94.9	
H.E.S.S.	1800	20	180	20	84.1	-16.2%
Beaufort West	1800	20	180	22	100.3	
H.E.S.S.	1800	40	0	37	89.4	-33.4%
Beaufort West	1800	40	0	45	134.3	
H.E.S.S.	1800	40	180	37	130.1	-1.3%
Beaufort West	1800	40	180	37	128.4	

Table 4.4: Energy threshold E_T, effective detection area A_{eff} of the sites of H.E.S.S. and Beaufort West as well as the difference of the effective detection area ΔA_{eff} between both sites.

H.E.S.S. and Beaufort West are both in the south of Africa. They have almost the same magnetic field, just the declination varies by $10.45°$, being $-13.62°$ for H.E.S.S. and $-24.07°$ for Beaufort West. Hence, the energy threshold and the effective detection area of both locations should be nearly the same. Table 4.4 contains the energy threshold E_T, the effective detection area A_{eff} at the H.E.S.S. site and Beaufort West as well as the difference in the effective detection area ΔA_{eff} between the two sites. Taking account of the errors in the energy threshold and the effective detection area, we could say that Beaufort West at an elevation of 2000 m has almost the same energy spectra, thresholds and effective detection areas as the site of H.E.S.S. The same can be seen in Figure 4.12(a) and 4.12(b).

(a) $\Theta = 20°$ (b) $\Theta = 40°$
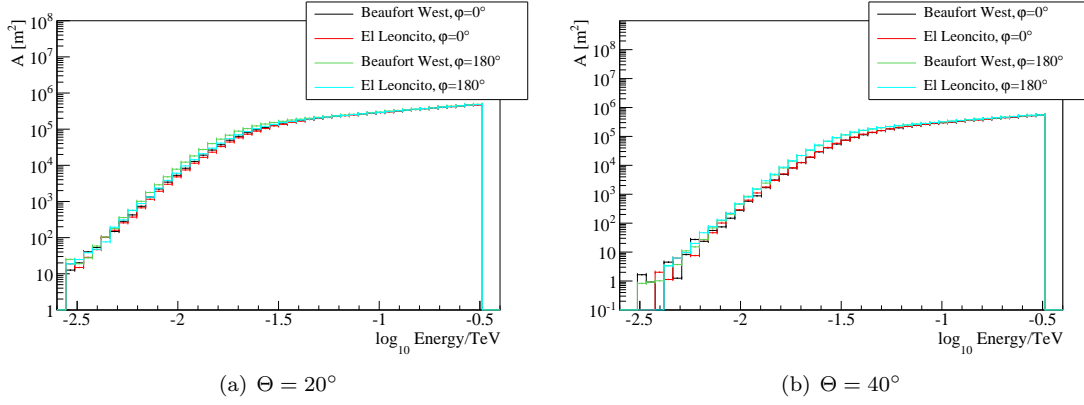
Figure 4.13: Comparison of the effective detection area at Beaufort West and El Leoncito at an altitude of 2000 m for azimuth angles φ at $0°$ and $180°$.

Site	Altitude h	Zenith Θ	Azimuth φ	E_T	A_{eff}	ΔA_{eff}
	[m]	[°]	[°]	[GeV]	[1000 m^2]	
Beaufort West	2000	20	0	22	81.5	11.1%
El Leoncito	2000	20	0	25	91.7	
Beaufort West	2000	20	180	20	85.2	2.4%
El Leoncito	2000	20	180	22	87.3	
Beaufort West	2000	40	0	41	117.2	1.3%
El Leoncito	2000	40	0	41	118.8	
Beaufort West	2000	40	180	33	110.8	18.2%
El Leoncito	2000	40	180	37	135.5	
Beaufort West	1800	20	0	25	94.9	16.0%
El Leoncito	2500	20	0	22	81.8	
Beaufort West	1800	20	180	22	100.3	27.8%
El Leoncito	2500	20	180	20	78.5	
Beaufort West	1800	40	0	45	134.3	5.3%
El Leoncito	2500	40	0	41	127.6	
Beaufort West	1800	40	180	37	128.4	1.1%
El Leoncito	2500	40	180	33	127.0	

Table 4.5: Energy threshold E_T, effective detection area A_{eff} of the sites of Beaufort West and El Leoncito as well as the difference of the effective detection area ΔA_{eff} between both sites.

In comparison to these both locations, El Leoncito shows almost the same behaviour at 2000 m but especially at low energies (3-5 GeV) its effective area is smaller than that of Beaufort West because the influence of the geomagnetic field is larger at El Leoncito (Figure 4.13(a) and 4.13(b)). In Table 4.5 the values of E_T, $A_{eff}(E_T)$ and ΔA_{eff} are compiled. From the error of E_T results an uncertainty of A_{eff} of about $20 \cdot 10^3 \ m^2$. The differences ΔA_{eff} are almost in all cases smaller than the uncertainties of $A_{eff}(E_T)$, hence the values of ΔA_{eff} represent more a tendency than a hard criterion.

(a) $\Theta = 20°$　　　　　　　　(b) $\Theta = 40°$
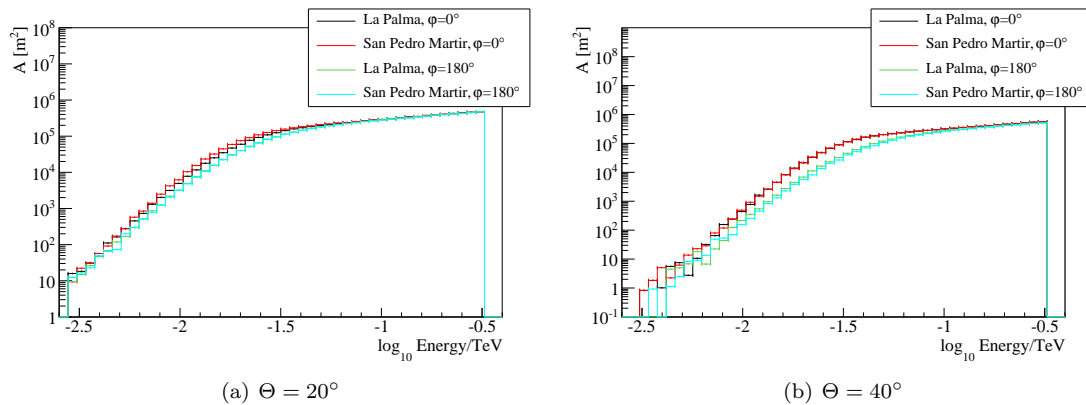
Figure 4.14: Comparison of the effective detection area of the detected showers at La Palma and San Pedro Martir at an altitude of 2000 m for azimuth angles φ at $0°$ and $180°$.

Site	Altitude h	Zenith Θ	Azimuth φ	E_T	A_{eff}	ΔA_{eff}
	[m]	[°]	[°]	[GeV]	[1000 m^2]	
La Palma	2000	20	0	22	78.1	3.0%
San Pedro Martir	2000	20	0	20	75.8	
La Palma	2000	20	180	25	69.9	-14.8%
San Pedro Martir	2000	20	180	27	82.0	
La Palma	2000	40	0	33	111.4	-17.8%
San Pedro Martir	2000	40	0	37	135.5	
La Palma	2000	40	180	50	119.7	58.3%
San Pedro Martir	2000	40	180	41	75.6	
La Palma	2200	20	0	22	80.9	34.8%
San Pedro Martir	3000	20	0	20	60.0	
La Palma	2200	20	180	27	85.8	39.1%
San Pedro Martir	3000	20	180	18	61.7	
La Palma	2200	40	0	33	115.5	42.8%
San Pedro Martir	3000	40	0	37	80.9	
La Palma	2200	40	180	45	106.7	43.4%
San Pedro Martir	3000	40	180	30	74.4	

Table 4.6: Energy threshold E_T, effective detection area A_{eff} of the sites of La Palma and San Pedro Martir as well as the difference of the effective detection area ΔA_{eff} between both sites.

The comparison between the site of La Palma and San Pedro Martir is illustrated in Figure 4.14(a) and 4.14(b). At an azimuth angle of 0° and a zenith of 20° and 40° San Pedro Martir shows larger effective detection areas than La Palma because the absolute value of the vertical component of the geomagnetic field strength is smaller at the site of San Pedro Martir. At an azimuth of 180° the effective detection areas are slightly larger at La Palma. This is in accordance with the expectation from the geomagnetic field strength. On the other hand, the impact of the geomagnetic field at San Pedro Martir is larger than at La Palma. The energy spectra for all four directions at La Palma are closer together because the influence of the geomagnetic field on the shower development is smaller. Table 4.6 lists the values of the energy threshold and the effective detection areas calculated at E_T.

4.3.3 Reduction of energy threshold

A method of reducing the energy threshold is to operate the telescope at a higher altitude. A reduction in distance to the shower maximum would increase the density of Cherenkov light at the observatory level. Thus, the installation of CTA at high altitudes would allow a reduction of the energy threshold

[10, 28]. As an example: If we take a particle shower with a shower maximum at $z_{max} = 10\ km$, one site with an altitude of $h_1 = 3\ km$ (San Pedro Martir) and another site at an altitude of $h_2 = 2.2\ km$ (La Palma), we obtain for the ratio of the square of the average light paths, F:

$$F = \left(\frac{z_{max} - h_2}{z_{max} - h_1} \right)^2 = 1.24. \tag{4.4}$$

The density of light at San Pedro Martir would be about 1.24 times higher than that at La Palma (Appendix D). The energy threshold would be reduced by the same factor of ∼1.24. However, the effective detection area would decrease, too. The calculation for the locations of El Leoncito ($h_1 = 2.5\ km$) and Beaufort West ($h_2 = 1.8\ km$) would result in a factor of 1.2 too. Hence, compared to Beaufort West (1800 m) and La Palma (2200 m), El Leoncito (2500 m) in the southern hemisphere and San Pedro Martir (3000 m) in the northern hemisphere have lower energy thresholds but smaller effective areas (Appendix G and I). Tables 4.4 - 4.6 list the values of these quantities. This tradeoff makes this comparison difficult. For a decision of the position of CTA it is important that the energy threshold of the location is as small as possible and the effective detection area is as large as possible.

Chapter 5

Conclusion & Outlook

The aim of this work was to quantify the influence of the strength and the direction of the geomagnetic field at the different possible locations on the sensitivity of the Cherenkov Telescope Array using Monte Carlo simulations of photon induced particle showers. The simulation tools CORSIKA and sim_telarray were used. We obtained results on the lateral distribution of Cherenkov photons on ground, the energy threshold and the effective detection area. After the study of the influence of the geomagnetic field of all twelve candidate sites at an altitude of 2000 m, we decided in favour of the following sites which we analysed in detail:

- Southern hemisphere: Beaufort West (South Africa), El Leoncito (Argentina), H.E.S.S. (Namibia)

- Northern hemisphere: La Palma (Canary Island), San Pedro Martir (Mexico)

It is important to note that the density of Cherenkov photons on the ground depends on the direction the particle shower comes from and the altitude of the candidate site. For locations in the southern hemisphere the density of Cherenkov photons on the ground is larger if the particle approaches ground at an azimuth angle of 180° (from the south to the north). The density is smaller for the opposite direction. The difference in photon density at ground level is from about 17% to 6% at the site Beaufort West and from about 22% to 5% at the position of El Leoncito. For locations in the northern hemisphere the density of Cherenkov photons at ground level describes the opposite situation. At an azimuth angle of 180° the density is smallest and at 0° it is largest. The variation amounts from 10% to 40% on the Canary Island La Palma and from about 15% to 50% at the position of San Pedro Martir. The minimum influence of the geomagnetic field on the shower development is at the site of Beaufort West in the southern hemisphere and at the position of the Canary Island La Palma in the northern hemisphere. Here the distribution of the Cherenkov photons at ground level agrees very well with a location without geomagnetic field.

Furthermore, we calculated the effective detection areas at the positions of the maximum value of the energy spectra, E_T, of detected photons. For locations in the southern hemisphere E_T is smallest if the observation takes place at an azimuth angle of 180° and largest at an azimuth of 0°. For the locations stationed in the southern hemisphere the following values for E_T are obtained:

Site	Altitude	Zenith	Azimuth	E_T
	[m]	[°]	[°]	[GeV]
H.E.S.S	2000	20	0	25
	2000	20	180	20
	2000	40	0	37
	2000	40	180	33
Beaufort West	2000	20	0	22
	2000	20	180	20
	2000	40	0	41
	2000	40	180	33
El Leoncito	2000	20	0	25
	2000	20	180	22
	2000	40	0	41
	2000	40	180	37

Table 5.1: Energy threshold E_T for the locations in the southern hemisphere at a fictitious altitude of 2000 m.

Estimated in the northern hemisphere the behaviour of the energy threshold is opposite. At an azimuth angle of 180° the energy threshold is largest and at 0° is smallest. The following values are obtained:

Site	Altitude	Zenith	Azimuth	E_T
	[m]	[°]	[°]	[GeV]
La Palma	2000	20	0	22
	2000	20	180	25
	2000	40	0	33
	2000	40	180	50
San Pedro Martir	2000	20	0	20
	2000	20	180	27
	2000	40	0	37
	2000	40	180	41

Table 5.2: Energy threshold E_T for the locations in the northern hemisphere at a fictitious altitude of 2000 m.

In summary, Beaufort West in the southern hemisphere and La Palma in the northern hemisphere have the smallest energy thresholds, e.g. the greatest sensitivity on gamma-ray sources.

After the study of the effective detection areas, we obtained the following results. In accordance with the results of the energy thresholds, the effective detection areas at the locations in the southern hemisphere are largest at an azimuth angle of 180° and smallest at 0°. The candidate sites in the northern hemisphere are characterised by the opposite situation. The effective detection areas estimated at a zenith angle of 20° are larger than at a zenith angle of 40°. To sum up, the effective detection areas are largest for Beaufort West in the southern hemisphere; and La Palma ($\varphi = 180°$) and San Pedro Martir ($\varphi = 0°$) in the northern hemisphere.

In conclusion, the geomagnetic field has the minimum influence on the shower development at the sites of Beaufort West in the southern hemisphere. In the northern hemisphere the situation is as follows. At an azimuth angle of 0° the minimum influence of the geomagnetic field occurs at San Pedro Martir and at 180° at the Canary Island La Palma.

It is important to know that the disadvantages of the candidate sites El Leoncito and San Pedro Martir resulting from a large influence of the geomagnetic field are compensated by a higher altitude of the locations. The density of Cherenkov photons increases from about 25% to 40% between San Pedro Martir and La Palma in the northern hemisphere. The energy threshold and the effective detection area would be reduced by a factor of about 1.24. In the southern hemisphere the variation in the density of Cherenkov photons between the locations of El Leoncito and Beaufort West is about 15% to 40%. The factor in the reduction of the energy threshold and the effective detection area is about 1.2.

After the investigation of the Cherenkov light characteristics, the energy spectra and the corresponding effective detection areas, we chose as place for the southern array and as place for the northern array:

- El Leoncito in Argentina

- San Pedro Martir in Mexico

Quoted according to the CTA consortium [16] the final decision of a location for CTA should be as follows:

> „The final decision among otherwise identical sites may rely on considerations such as financial or in-kind contributions by the host regions. It is likely that an inter-governmental agreement will be required to assure long-term availability of the site, as well as guaranteed access and free transfer of data. At the same level, issues such as import taxes, value added tax and fees etc. should be addressed. Such agreements exist, for H.E.S.S., Auger and other observatories operated by international collaborations."

Appendix

A Simulation of the Cherenkov light characteristics

RUNNR	102409	run number
EVTNR	1	number of first shower event
NSHOW	2500	number of showers to generate
PRMPAR	1	particle type of primary particle
ERANGE	100. 100.	energy range of primary particle (GeV)
ESLOPE	-2.	slope of primary energy spectrum
THETAP	40. 40.	range of zenith angle (degree)
PHIP	90. 90.	range of azimuth angle (degree)
ARRANG	-13.62	rotation of array to north
OBSLEV	2000.E2	observation level (cm)
ATMOD	1	number of atmospheric parametrization
MAGNET	12.190 -25.684	magnetic field (horizontal and vertical component) (μT)
ELMFLG	F T	electromagnetic interaction steering flag (NKG disabled, EGS4 selected)
RADNKG	200.E2	outer radius (cm) for NKG lateral density distribution
FIXCHI	0.	starting altitude (g/cm^2)
QGSJET	T 0	QGSJET for high energy and debug level
QGSSIG	T	QGSJET cross-sections enabled
URQMD	T 0	Low energy model
HILOW	100.	transition energy between low and high energy hadronic interaction model (GeV)
ECUTS	0.30 0.05 0.02 0.02	Energy Cut-Offs
MUMULT	T	muon multiple scattering angle
LONGI	T 20. F F	longitudinal distribution, step size (g/cm^2), fit, out
MAXPRT	50	maximum number of printed events
ECTMAP	1.E5	cut on gamma factor for printout
DEBUG	F 6 F 1000000	debug flag, logarithmic unit, delayed debug
DIRECT	/batch/2171808.1.12h.q/	directory of particle output
USER	mkrause	user name for the data base file
HOST	blade88.ifh.de	host name for the data base file
ATMOSPHERE	1 Y	tropical atmosphere with atmospheric refraction for Cherenkov Photons
CERARY	1 1 1 1 100000 100000	Cherenkov detector grid (cm)
CERFIL	T	Cherenkov output file
CERQEF	F T F	no quantum efficiency of detector photomultiplier, atmospheric absorption of Cherenkov Photons, no mirror reflectivity of Cherenkov

		telescopes
CERSIZ	5.	bunch size of Cherenkov photons
CWAVLG	250. 700.	Cherenkov wavelength band (nm)
EXIT		terminates input

Table 5.3: CORSIKA Input card for the analysis of the Cherenkov light characteristics.

B Simulation of the Extensive Air Showers

RUNNR	224	run number
EVTNR	1	number of first shower event
NSHOW	50000	number of showers to generate
DATBAS	no	write a file with parameters used
ESLOPE	-2.	slope of primary energy spectrum
THETAP	40. 40.	range of zenith angle (degree)
PHIP	90. 90.	range of azimuth angle (degree)
PRMPAR	1	particle type of primary particle
VIEWCONE	0. 0.	can be a cone around fixed THETAP/PHIP
CSCAT	10 500E2 0.	use shower several times (gammas), maximum scattering of core location in a circle of radius XSCATT if $YSCATT = 0$
ERANGE	3. 300	energy range of primary particle (GeV)
OBSLEV	2000.E2	observation level (cm)
MAGNET	12.0 -26.0	magnetic field (horizontal and vertical component) (μT)
ARRANG	-13.62	rotation of array to north
FIXHEI	0. 0.	first interaction height & target
FIXCHI	0.	starting altitude (g/cm^2)
TSTART	T	needed for emission and scattering of primary particle
ECUTS	0.30 0.1 0.020 0.020	Energy Cut-Offs
MUMULT	T	muon multiple scattering angle
LONGI	T 20. F F	longitudinal distribution, step size (g/cm^2), fit, out
MAXPRT	0	maximum number of printed events
ECTMAP	1.E6	cut on gamma factor for printout
STEPFC	1.0	multiple scattering step length factor
CERSIZ	5.	bunch size of Cherenkov photons
CWAVLG	250. 700.	Cherenkov wavelength band (nm) delayed debug
DIRECT	/dev/null	directory of particle output; /dev/null means no normal CORSIKA data written
USER	mkrause	user name for the data base file
HOST	blade88.ifh.de	host name for the data base file
EXIT		terminates input

Table 5.4: CORSIKA Input card for the analysis of Extensive Air Showers.

C Lateral distribution of the Cherenkov photon density at an altitude of 2000 m
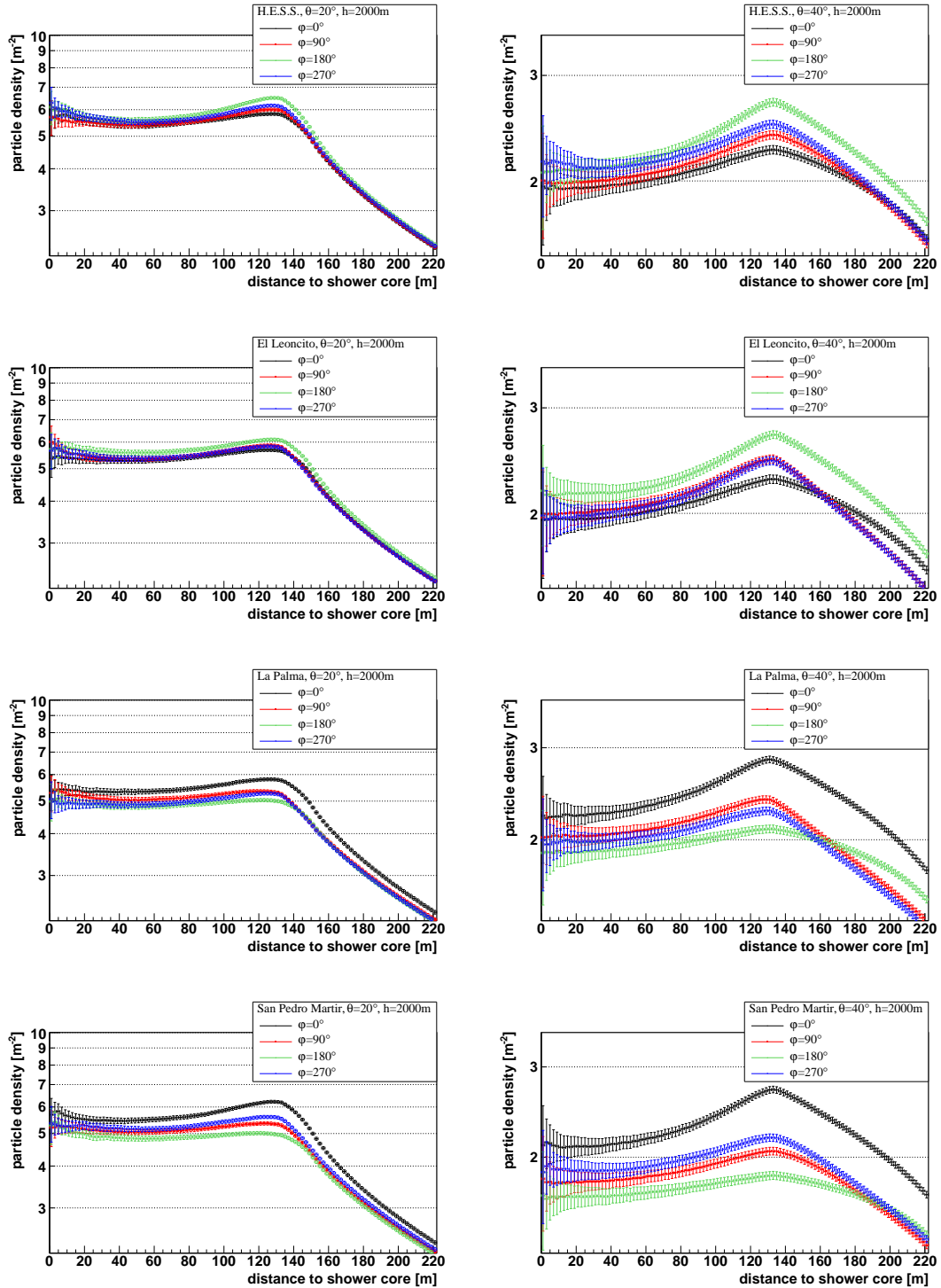
Figure C1: Lateral distribution of the density of 250-700 nm Cherenkov photons in simulations of 100 GeV gamma-rays for the sites of H.E.S.S., El Leoncito, La Palma and San Pedro Martir (2000 m) for zenith angles Θ at $20°$ and $40°$ and azimuth angles φ at $0°$, $90°$, $180°$ and $270°$.

D Lateral distribution of the Cherenkov photon density at the specific altitudes
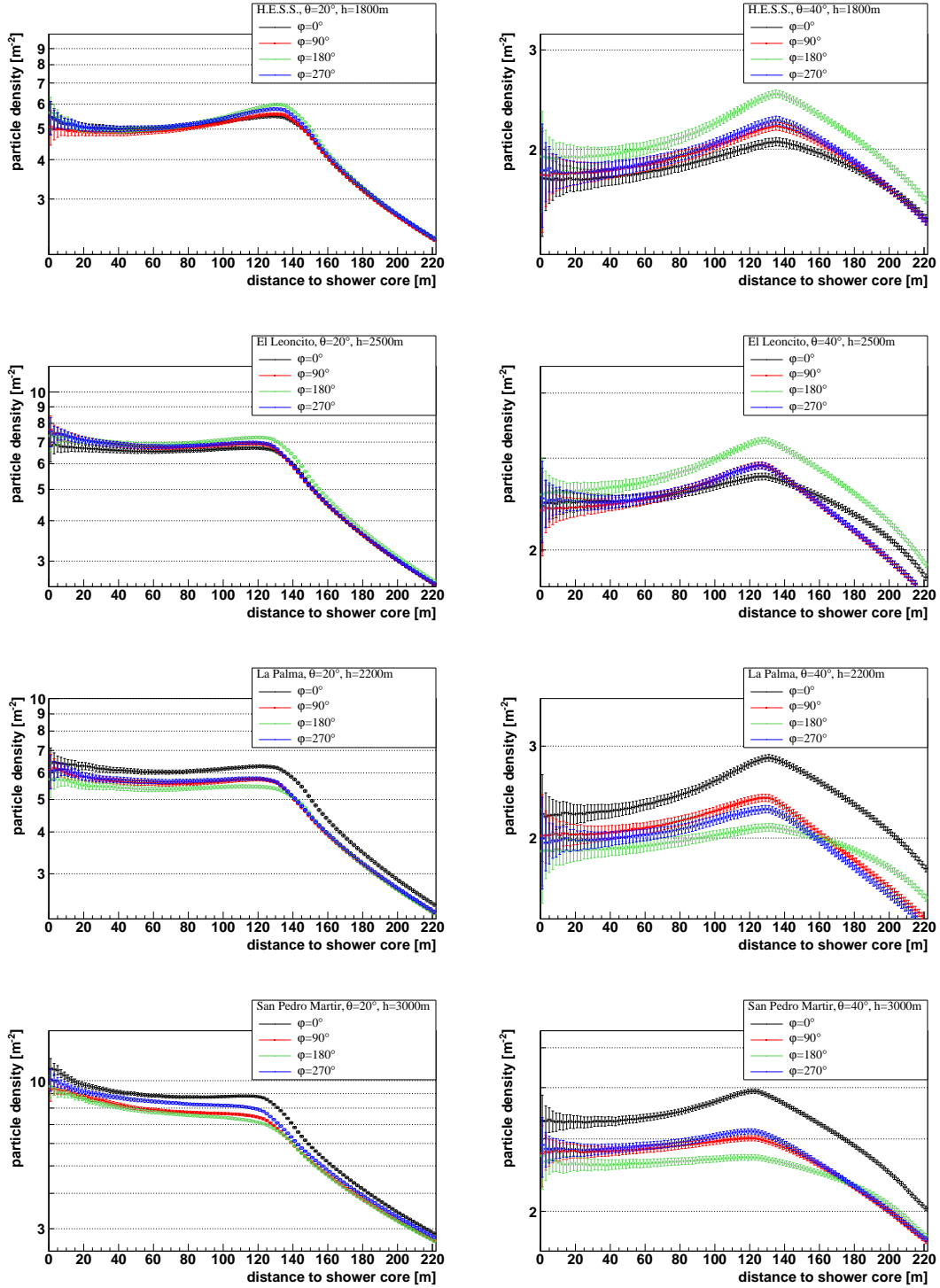
Figure D2: Lateral distribution of the density of 250-700 nm Cherenkov photons in simulations of 100 GeV gamma-rays at the sites of H.E.S.S. (1800 m), El Leoncito (2500 m), La Palma (2200 m) and San Pedro Martir (3000 m) for zenith angles Θ at 20° and 40° and azimuth angles φ at 0°, 90°, 180° and 270°.

E Lateral distribution of the Cherenkov photon density at the considered sites at a fictitious altitude of 2000 m in comparison to B=0
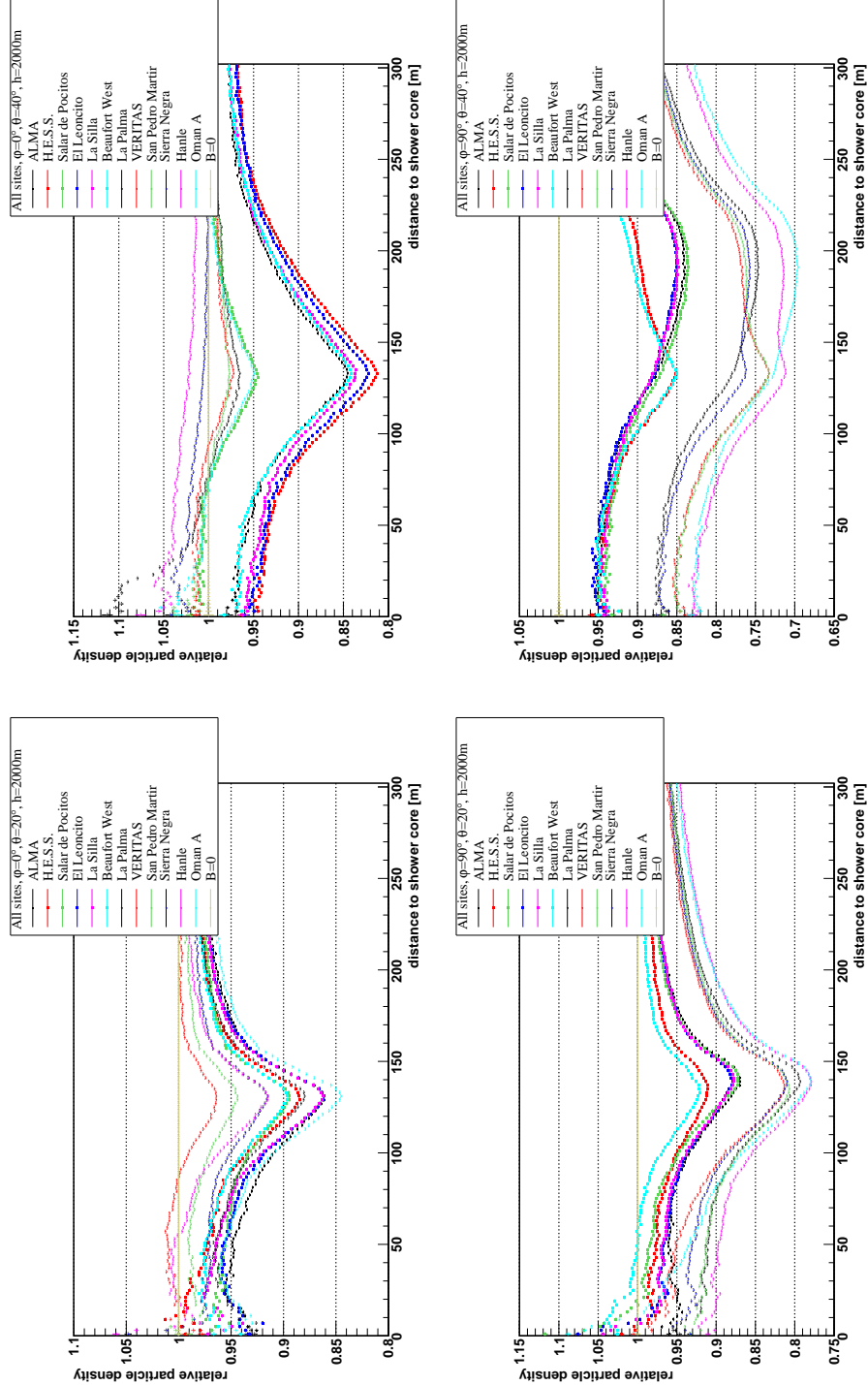
Figure E3: Lateral distribution of the density of 250-700 nm Cherenkov photons normalised to the density obtained for B=0. The photon energy is 100 GeV and all sites are assumed at 2000 m. Zenith angles Θ at 20° and 40° and azimuth angles φ of 0° and 90°.
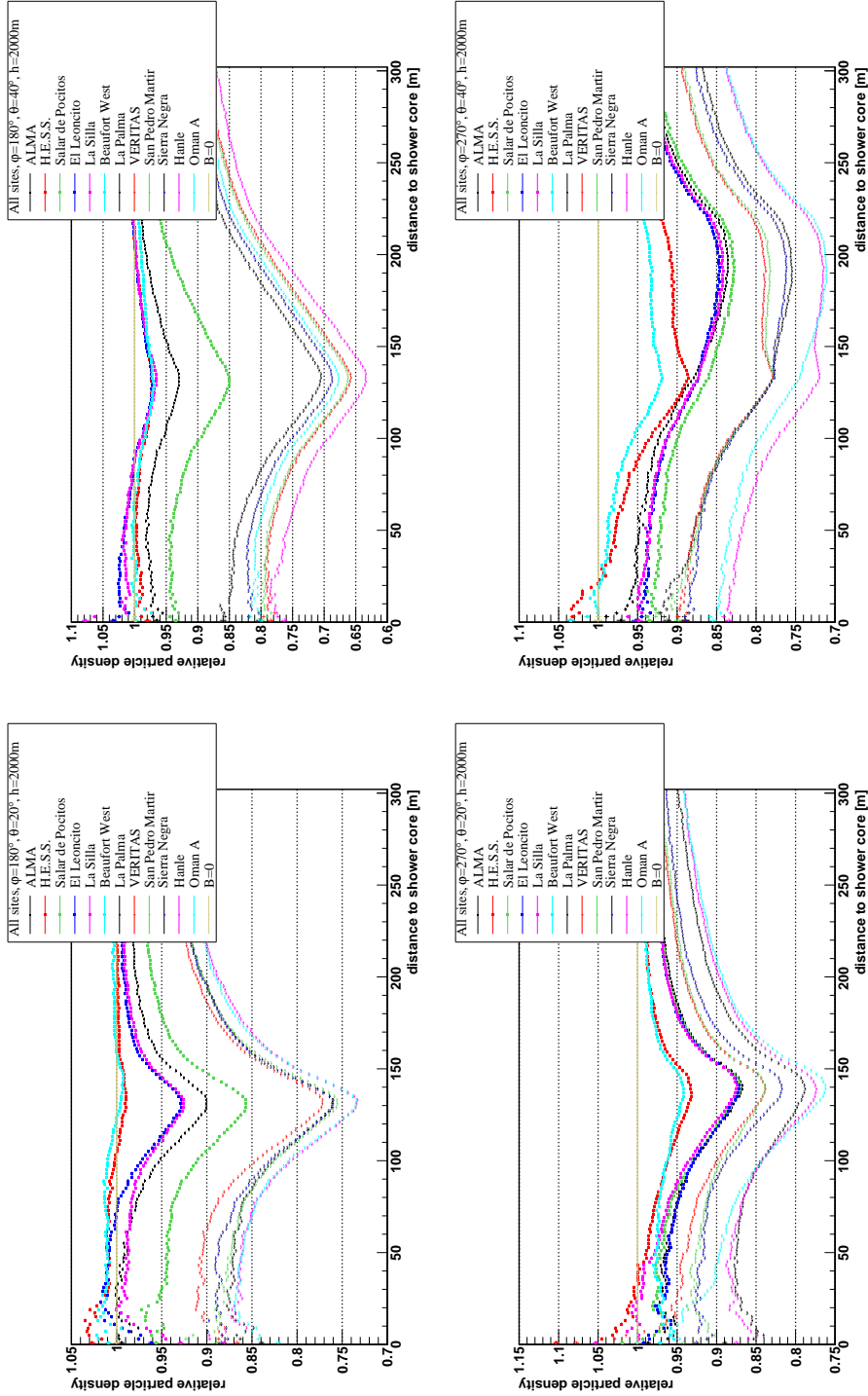
Figure E4: Lateral distribution of the density of 250-700 nm Cherenkov photons normalised to the density obtained for B=0. The photon energy is 100 GeV and all sites are assumed at 2000 m. Zenith angles Θ at 20° and 40° and azimuth angles φ of 180° and 270°.

F Generated and reconstructed photon energy spectra at an altitude of 2000 m
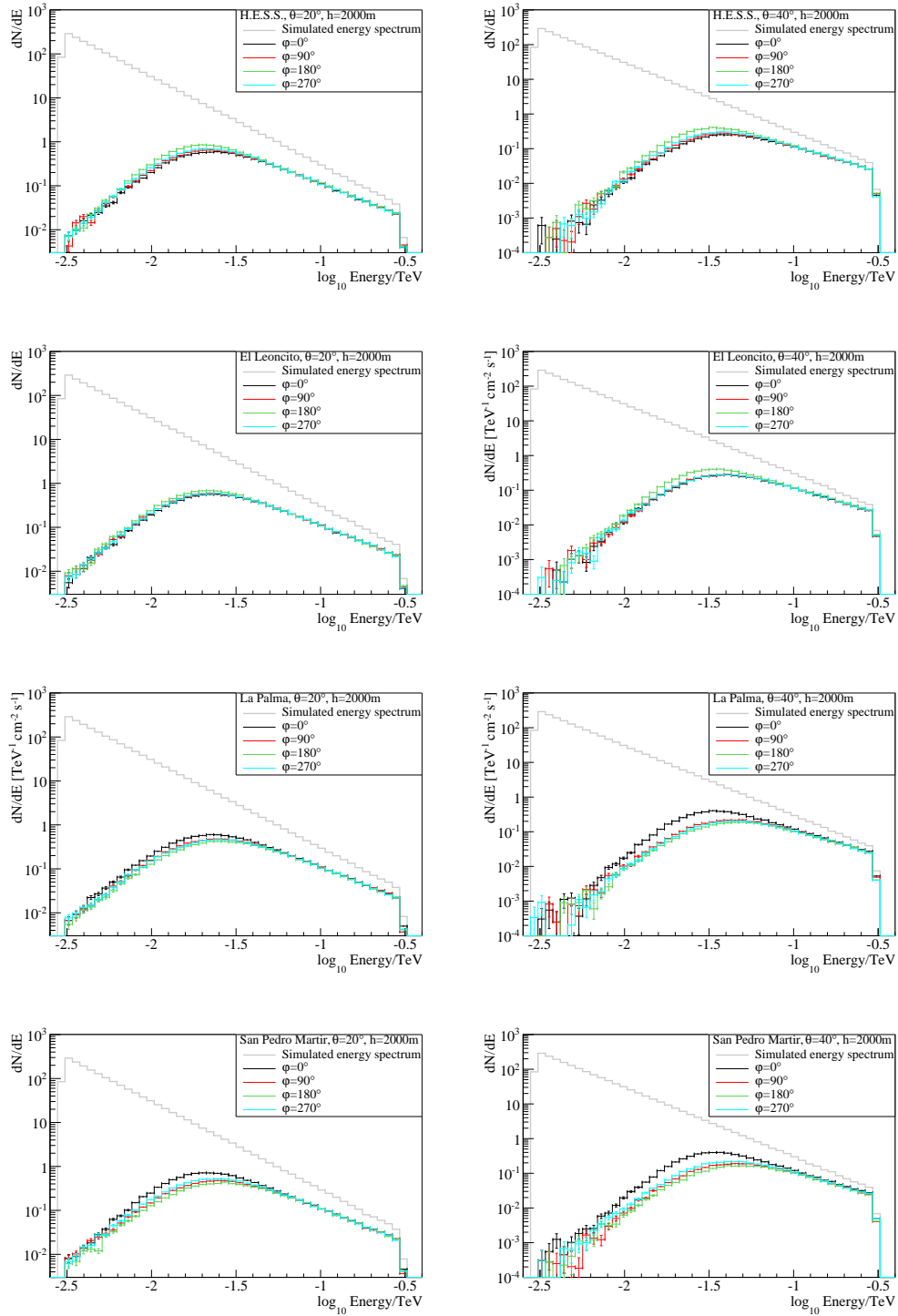
Figure F5: Energy spectra of the generated and reconstructed photons of gamma-rays between 3 GeV to 300 GeV at the sites of H.E.S.S., El Leoncito, La Palma and San Pedro Martir (2000 m) for zenith angles Θ at 20° and 40° and azimuth angles φ at 0°, 90°, 180° and 270°.

G Generated and reconstructed photon energy spectra at the specific altitudes
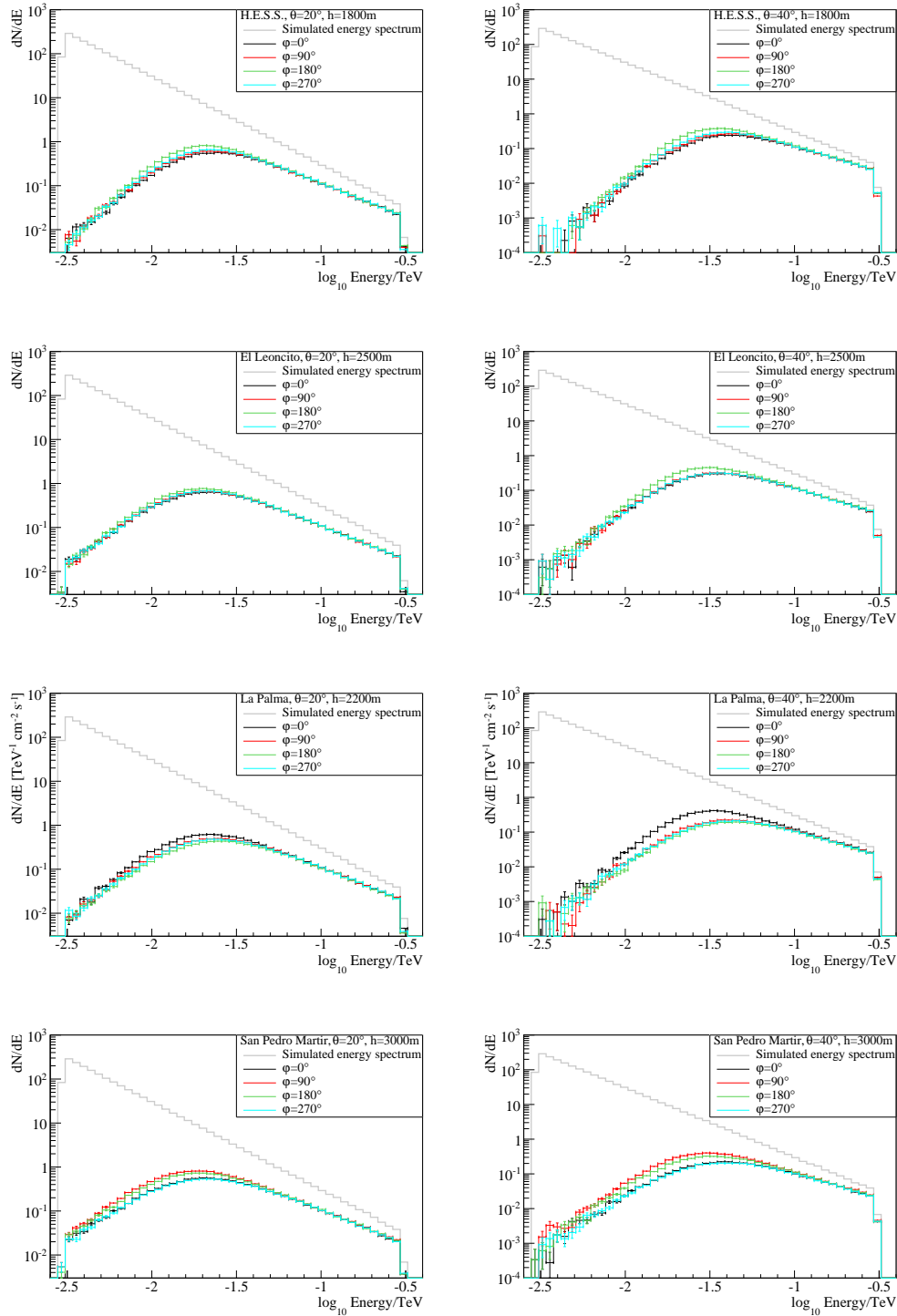
Figure G6: Energy spectra of the generated and reconstructed photons of gamma-rays between 3 GeV to 300 GeV at the sites of H.E.S.S. (1800 m), El Leoncito (2500 m), La Palma (2200 m) and San Pedro Martir (3000 m) for zenith angles Θ at 20° and 40° and azimuth angles φ at 0°, 90°, 180° and 270°.

H Effective detection area for all sites at an altitude of 2000 m
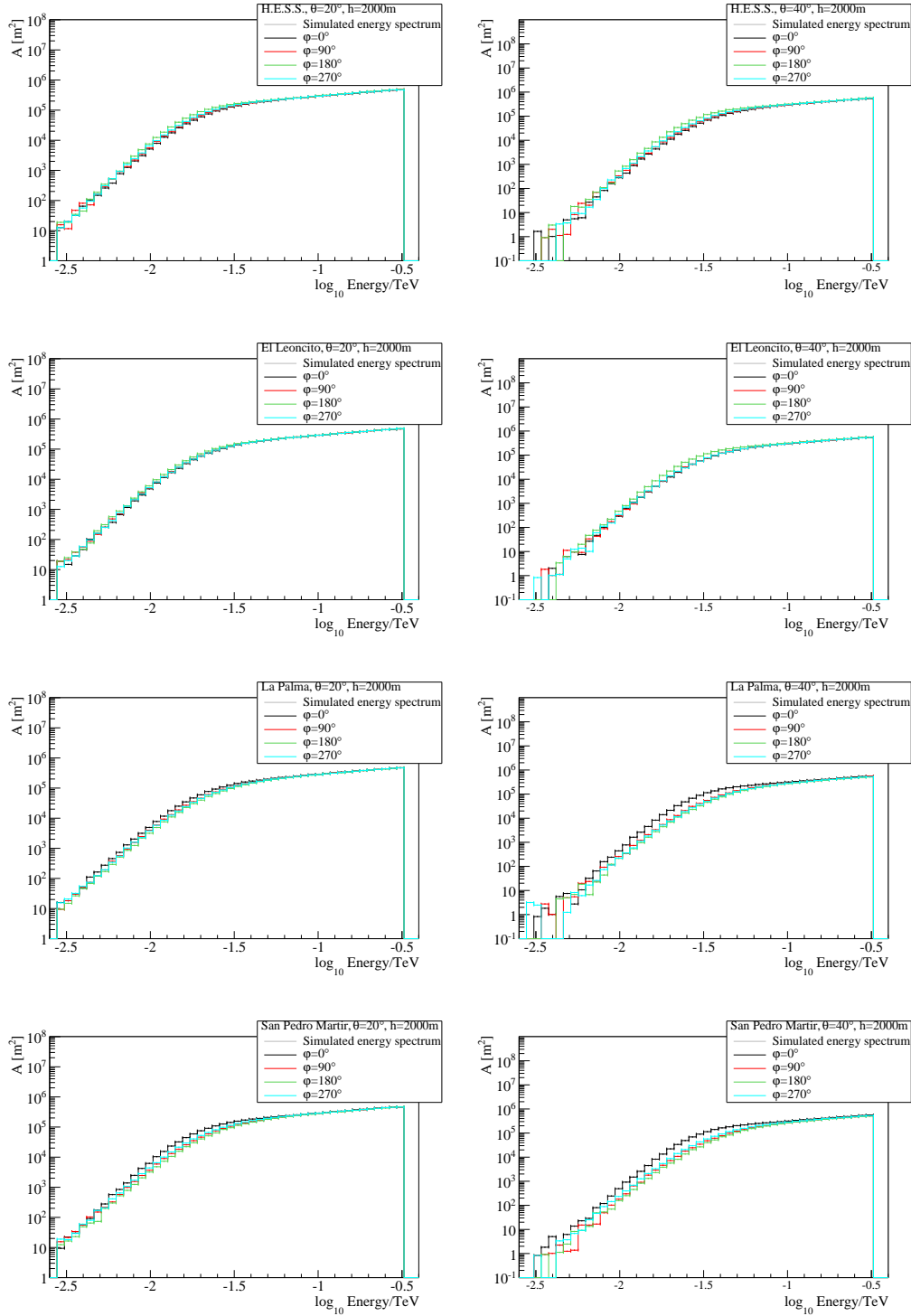
Figure H7: Effective detection area of gamma-rays between 3 GeV to 300 GeV at the sites of H.E.S.S., El Leoncito, La Palma and San Pedro Martir (2000 m) for zenith angles Θ at 20° and 40° and azimuth angles φ at 0°, 90°, 180° and 270°.

I Effective detection area for all sites at the specific altitudes
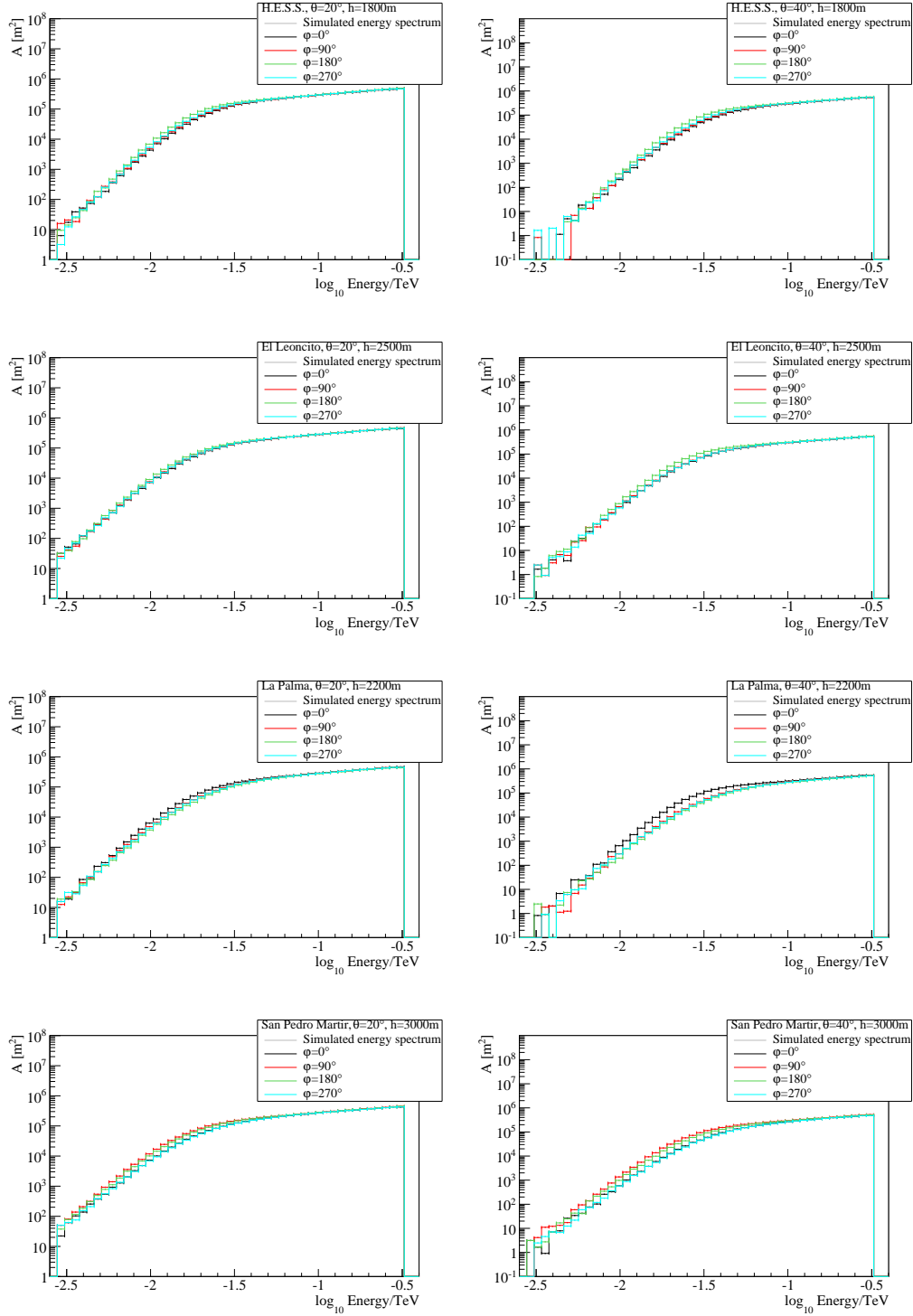
Figure I8: Effective detection area of gamma-rays between 3 GeV to 300 GeV at the sites of H.E.S.S. (1800 m), El Leoncito (2500 m), La Palma (2200 m) and San Pedro Martir (3000 m) for zenith angles Θ at $20°$ and $40°$ and azimuth angles φ at $0°$, $90°$, $180°$ and $270°$.

Bibliography

[1] T. Weekes. Very High Energy Gamma-Ray Astronomy. Institute of Physics Publishing: Bristol and Philadelphia, 2003.

[2] E. Lorenz. High-energy astroparticle physics. In *Nuclear Instruments and Methods in Physics Research Section A* , 567: 1-11, 2006.

[3] C. Grupen. Astroteilchenphysik. Vieweg: Braunschweig/ Wiesbaden, 2000.

[4] C. Grupen. Teilchendetektoren. Bibliographisches Institut-Wissenschaftsverlag: Mannheim, 1993.

[5] Particle Data Group. Particle Physics Booklet, July 2010.

[6] W. Lohmann. Script to the lecture *Allgemeine Physik III - Kerne und Teilchen*. Brandenburg University of Technology, Summer semester 2009.

[7] H. A. Bethe. Molière's Theory of Multiple Scattering. In *Physical Review* , 89 (6): 1256-1266, 1953.

[8] CTA: Physics analysis and optimization of the CTA array performance with Monte Carlo methods found on 20th August 2010
http://nuastro-zeuthen.desy.de/cta/the_experiment/mc_phys/index_eng.html

[9] J. Matthews. A Heitler model of extensive air showers. In *Astroparticle Physics* , 22: 387-397, 2005.

[10] F. Aharonian, J Buckley, T. Kifune, G. Sinnis. High energy astrophysics with ground-based gamma ray detectors. In *Reports on Progress in Physics* , 71: 2008.

[11] A. Schönwald, U. Schwanke, Aufgabenstellung zum Praktikum *Tscherenkow-Strahlung in atmosphärischen Teilchenschauern* , 2007, unpublished.

[12] National Geographic Data Center (NGDC)
found on 28th July 2010
http://www.ngdc.noaa.gov/geomag/

[13] H. Kolanoski. Script to the lecture *Einführung in die Astroteilchenphysik*. Institut für Physik, Humboldt-Universität zu Berlin, Wintersemester 2006/ 2007.

[14] V. Haak, M. Korte, I. Wardinski. Das ruhelose Magnetfeld der Erde - Was wir über den Geodynamo wissen. In: *Sterne und Weltraum* , 45: 22-31, 6/2006.

[15] Cherenkov Telescope Array: An advanced facility for ground-based gamma-ray astronomy found on 20th August 2010
http://www.cta-observatory.org/

[16] W. Hofmann, M. Martinez. Design Concepts for the Cherenkov Telescope Array CTA - An Advanced Facility for Ground-Based High-Energy Gamma-Ray Astronomy. The CTA Consortium: May 2010.

[17] CTA: An Advanced Facility for High-Energy Gamma-Ray Astronomy
found on 20th August 2010
http://nuastro-zeuthen.desy.de/cta/index_eng.html

[18] G. Bohm, G. Zech. Introduction to Statistics and Data Analysis for Physicists. In *Verlag Deutsches Elektronen-Synchrotron*: 2010.

[19] K. Binder, D. W. Heermann. Monte Carlo Simulation in Statistical Physics - An Introduction. Springer: Berlin, 2002.

[20] D. Heck, J. Knapp, J. N. Capdevielle, G. Schatz, T. Thouw. CORSIKA: A Monte Carlo Code to Simulate Extensive Air Showers. Forschungszentrum Karlsruhe GmbH, Karlsruhe (Germany), FZKA 6019, 1998.
CORSIKA version 6.735.

[21] D. Heck, T. Pierog. Extensive Air Shower Simulation with CORSIKA: A User's Guide. Karlsruher Institut für Technologie, Karlsruhe (Germany). 1998.

[22] W. R. Nelson, H. Hirayama, D. W. O. Rogers. The EGS4 Code System. SLAC, Stanford University, Stanford (California). 1985.

[23] S. C. Commichau, A. Biland, D. Kranich, R. de los Reyes, A. Moralejo, D. Sobczyńska. Geomagnetic Field Effects on the Imaging Air Shower Cherenkov Technique. In *Proceedings of the 30th International Cosmic Ray Conference* , Volume 3: 1357-1360, 2008.

[24] K. Bernlöhr. CTA simulations with CORSIKA/ sim_telarray. In *Proceedings of the 4th International Meeting on High Energy Gamma-Ray Astronomy* , Heidelberg: 874-877, 2008.

[25] K. Bernlöhr. Simulation of Imaging Atmospheric Cherenkov Telescopes with CORSIKA and sim_telarray. In *Astroparticle Physics* , 30: 149-158, 2008.

[26] S. C. Commichau, A. Biland, J. L. Contreras, R. de los Reyes, A. Moralejo, J. Sitarek, D. Sobczyńska. Monte Carlo Studies of Geomagnetic Field Effects on the Imaging Air Cherenkov Technique for the MAGIC Telescope Site. In *Nuclear Instruments and Methods in Physics Research Section A* , 595: 572-586, 2005.

[27] R. Brun, F. Rademakers. ROOT - An Object-Oriented Data Analysis Framework: Users Guide 5.26. CERN: July 2007.

[28] F.A. Aharonian, A.K. Konopelko, H.J. Völk, H. Quintana. 5@5 - a 5 GeV energy threshold array of imaging atmospheric Cherenkov telescopes at 5 km altitude. In *Astroparticle Physics* : October 2000. [arXiv: astro-ph/0006163v]

[29] G. Mohanty, S. Biller, D.A. Carter-Lewis, D.J. Fegan, A.M. Hillas, R.C. Lamb,T.C. Weekes, M. West, J. Zweerink. Measurement of TeV gamma-ray spectra with the Cherenkov imaging technique. In *Astroparticle Physics* , 9: 15-43, 1998.

[30] S. Funk, G. Hermann, J. Hinton, D. Berge, K. Bernlöhr, W. Hofmann, P. Nayman, F. Toussenel, P. Vincent. The Trigger System of the H.E.S.S. Telescope Array. In *Astroparticle Physics* , 22: 285-296, 2004.

[31] W. Benbow. The Status and Perfomance of H.E.S.S. In *Proceedings of the 2nd International Symposium on High Energy Gamma Ray Astronomy* , Heidelberg: 611-616, 2004

The references to arXiv can be found at http://arxiv.org/ and the corresponding article ID.

Acknowledgement

Selbstständigkeitserklärung - Declaration of academic honesty

Hiermit erkläre ich, dass ich die vorliegende Arbeit selbstständig und nur unter Verwendung der angegebenen Quellen und Hilfsmittel angefertigt habe.

Cottbus, 11. Februar 2011

....
Maria Krause

Herewith I affirm that I did the present work by myself and only with the use of the stated references.

Cottbus, 11st February 2011

....
Maria Krause